DEFORMATION OF SNOW UNDER RIGID PLATES AT A CONSTANT RATE OF PENETRATION

Gunars Abele

March 1970

DA TASK 1T062112A13001

CORPS OF ENGINEERS, U.S. ARMY
COLD REGIONS RESEARCH AND ENGINEERING LABORATORY
HANOVER, NEW HAMPSHIRE

THIS DOCUMENT HAS BEEN APPROVED FOR PUBLIC RELEASE
AND SALE; ITS DISTRIBUTION IS UNLIMITED.

PREFACE

This study was conducted by Mr. Gunars Abele, Research Civil Engineer, Applied Research Branch (Mr. A.F. Wuori, Chief), Experimental Engineering Division (Mr. K.A. Linell, Chief), U.S. Army Cold Regions Research and Engineering Laboratory (USA CRREL).

The study was performed during 1966 at the Keweenaw Research Center, Houghton, Michigan. This report was published under DA Task 1T062112A13001, *Cold Regions Research–Applied Research and Engineering.*

The author expresses appreciation to the staff of the Keweenaw Research Center for their assistance during the experimental work at that facility and to Dr. W.M. Haas of Michigan Technological University for his helpful advice and suggestions during the course of the work.

The author also expresses appreciation to Mr. D.E. Nevel of USA CRREL, who gave valuable advice and suggestions during this study and the preparation of this report.

The contents of this report are not to be used for advertising, publication, or promotional purposes. Citation of trade names does not constitute an official endorsement or approval of the use of such commercial products.

CONTENTS

	Page
Introduction	1
Background	1
Physical characteristics of snow	1
Mechanical behavior of snow	4
Failure mechanism of snow	6
Description of experimental work	6
Method	6
Preparation of test samples	8
Test apparatus and equipment	8
Procedure	9
Results and discussion	11
Mechanical properties of test samples	11
Experimental results	13
Summary, conclusions, and recommendations	31
Literature cited	33
Selected bibliography	35
Appendix A. Development of theoretical equations	39
Appendix B. Test data and calculations	51
Appendix C. Selected, representative photographs	59
Appendix D. Schedule of tests performed	65
Abstract	67

ILLUSTRATIONS

Figure		
1.	Unconfined compressive strength vs time for various densities	2
2.	Unconfined compressive strength vs time for various temperatures	2
3.	Strength vs temperature	3
4.	Unconfined compressive strength vs density	3
5.	Maxwell-Voigt model	4
6.	Dashpot-Voigt model	4
7.	Young's modulus vs density	5
8.	Poisson's ratio vs density	5
9.	Young's modulus vs unconfined compressive strength	5
10.	Load-sinkage relations	6
11.	Two-dimensional case	7
12.	Sample container	8
13.	Container with test sample in compression press	9
14.	Unconfined compressive strength vs density	12
15.	Bearing capacity vs unconfined compressive strength	13
16.	Method used in presenting deformation vs depth data	14
17.	Vertical deformation at Y-axis (density = 0.30-0.31)	14
18.	Vertical deformation at Y-axis (density = 0.34-0.36)	15
19.	Vertical deformation at Y-axis (density = 0.38)	15
20.	Vertical deformation at Y-axis (density = 0.42-0.44)	16

CONTENTS (Cont'd)

ILLUSTRATIONS (Cont'd)

Figure — Page

21. Vertical deformation at Y-axis (density = 0.45-0.47) 16
22. Vertical deformation at Y-axis (density = 0.53-0.54) 17
23. Vertical deformation at Y-axis (density = 0.56; density = 0.59) 17
24. Width of deformation bulb as related to bearing plate size 18
25. Vertical deformation at initial failure vs depth for various snow densities 19
26. Bearing plate penetration vs pressure 20
27. Penetration at initial failure vs density 20
28. Penetration at initial failure vs relative density 22
29. Penetration at initial failure vs density numeric 22
30. Penetration at initial failure vs density 22
31. Penetration vs pressure 23
32. Penetration vs pressure as related to density 24
33. Penetration vs pressure as related to density and plate size 24
34. Penetration at initial failure vs pressure 25
35. Progressive snow failure 26
36. z/p vs z^2 27
37. p/z vs p^2 27
38. η vs χ, theoretical curve compared with experimental data 29
39. σ_i, k_1, and p_m vs density 30
40. Penetration vs pressure 30
41. Bearing capacity vs mat thickness 31

TABLE

Table

I. Summary of tests conducted 10

DEFORMATION OF SNOW UNDER RIGID PLATES AT A CONSTANT RATE OF PENETRATION

by

Gunars Abele

INTRODUCTION

The object of this study was to investigate experimentally the deformation of a snow mass under a concentrated load and to compare the results with available theoretical values. The effect of applied surface pressure and contact area on the depth of critical deformation in snow was studied to aid in the development of design criteria for snow roads and runways in the polar areas.

The present design criteria for snow pavement construction are based on certain assumptions, such as the nature and depth of the deformation of the pavement that occurs under load and Boussinesq stress distribution,[1 2] neither of which has been verified theoretically nor fully investigated experimentally. The required thickness of a snow pavement having certain known strength properties cannot be established unless the vertical extent of the effect of the applied load is known.

The actual snow pavement or foundation has three dimensions. From the literature it is apparent that the analysis of stress and deformation in a three-dimensional body is extremely difficult. Consequently, the solutions of all but a few of the three-dimensional problems of elasticity have proved to be unattainable, at least in simple form. Furthermore, since snow in most applications cannot be considered an elastic material, the problem is even more complex. Reducing the case to be studied to two dimensions simplifies the problem, and the results may provide a sufficiently good picture of the deformation in the corresponding three-dimensional case.

In this study experimental data were obtained on the deformation of snow of various densities by applying load at a constant rate of penetration with various sizes of bearing plates. The tests were conducted in such a manner that the two-dimensional case was simulated, although in a somewhat imperfect fashion. Because of lack of the rather expensive equipment required to record the actual stresses introduced at various points in the material under load, only the deformation data were obtained.

The development of the theoretical stress and deformation equations did not appear to result in satisfactory solutions and, therefore, was not completed.

BACKGROUND

Physical characteristics of snow

Dry snow consists of ice, water vapor, air, and impurities. After the deposition of snow on the ground, metamorphism begins.[3] At first, the constituent ice crystals of the highly permeable mass adhere only weakly at points of mutual contact. Gradually there is a change in the size and shape of the crystals and their intergranular bonds. At subfreezing temperatures, mass transfer takes place by vapor diffusion and surface diffusion; the crystals lose their original shape and tend to become spherical, while the ice bonds between them grow.[4] The strength of the snow mass is thus gradually increased. This phenomenon, known as *sintering* or *age hardening,* has been discussed by various authors.[3 4 5 6]

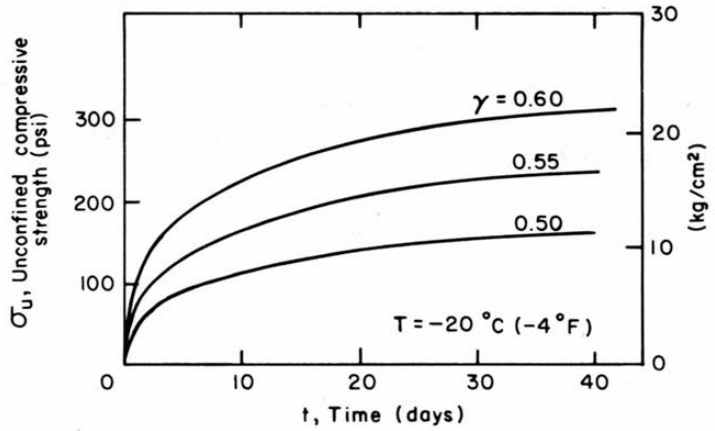

Figure 1. Unconfined compressive strength vs time for various densities. (After Ramseier.[6])

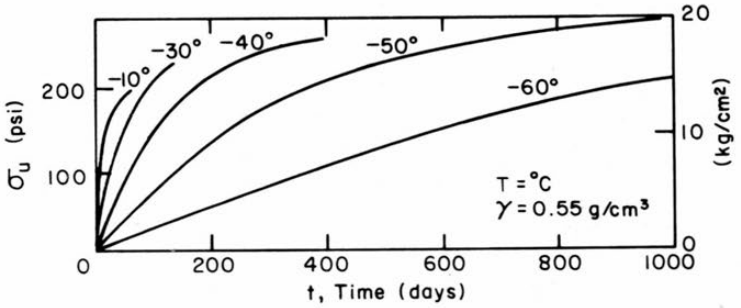

Figure 2. Unconfined compressive strength vs time for various temperatures. (After Ramseier.[6])

The sintering process can be accelerated considerably by mechanical agitation or disaggregation. If snow is milled (processed) with a rotary snowplow, such as the plows used in clearing highways, the density of snow is increased because of a more nonuniform particle size distribution and compaction; this results in a more intimate grain-to-grain contact. The increased number of these contacts per unit volume results in a more rapid bond growth between the closely packed grains.

By processing snow with a high-speed rotary snowplow, such as the Peter Snowmiller, and compacting it further immediately after processing, a high rate of sintering can be obtained.[7]

The sintering process produces an exponential increase in strength with time, the rate constant depending on temperature and grain characteristics. Figure 1 shows the strength increase as a function of time and initial density at a temperature of –20C (–4F). During the sintering process, the density of snow remains virtually constant.

The temperature during the sintering process has a very pronounced influence on the rate of sintering. Figure 2 shows that the rate of sintering decreases with a decrease in temperature. However, snow which is sintering at a lower temperature will ultimately reach a higher strength than

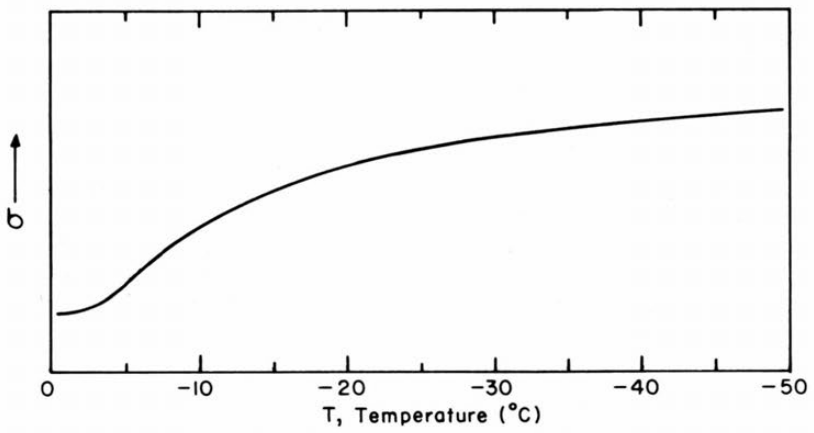

Figure 3. Strength vs temperature. (After Mellor.[4])

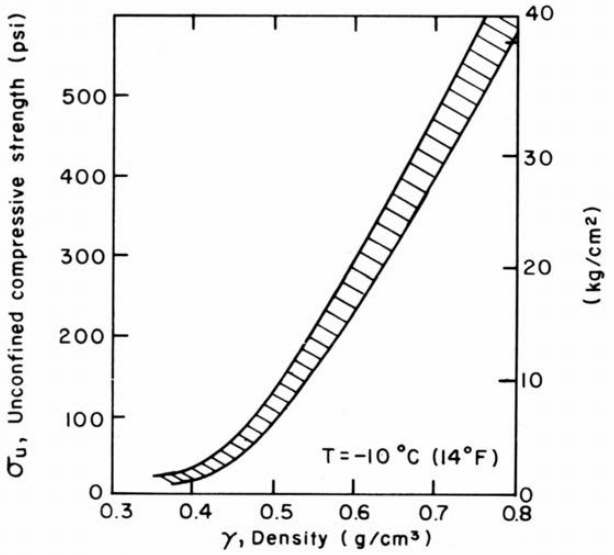

Figure 4. Unconfined compressive strength vs density. (After Mellor.[4])

snow which is sintering at a higher temperature and completes its sintering process in a shorter period of time. Everything else being equal, snow strength increases with a decrease in temperature (Fig. 3).

Snow disaggregated with a rotary snow miller has a density of approximately 0.5 g/cm.^{3} (Since density in the metric system is also equivalent to specific gravity in the British system, density data will be given only in metric units.) Further compaction can increase it to 0.6 g/cm^3 or more. Figures 1 and 4 show that for this density, unconfined strength equal to or exceeding the tire contact pressures of heavy aircraft can be obtained in a few weeks. It is concluded, therefore, that under favorable climatic conditions, snow pavement of such strength may be quite adequate for support of heavy wheel loads. This has been verified in simulated aircraft wheel load tests and on experimental runways.[2 8 9]

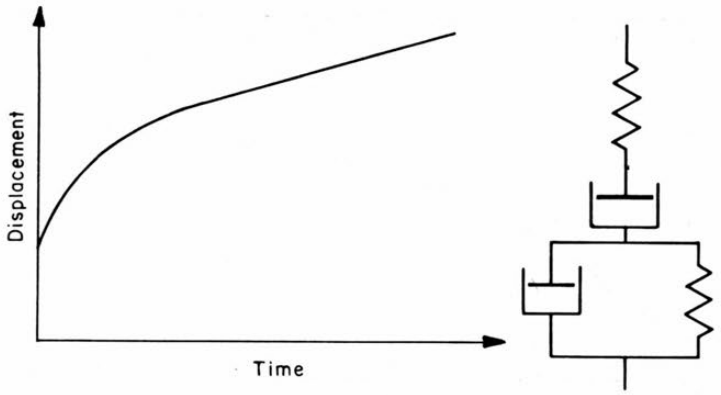

Figure 5. Maxwell-Voigt model.

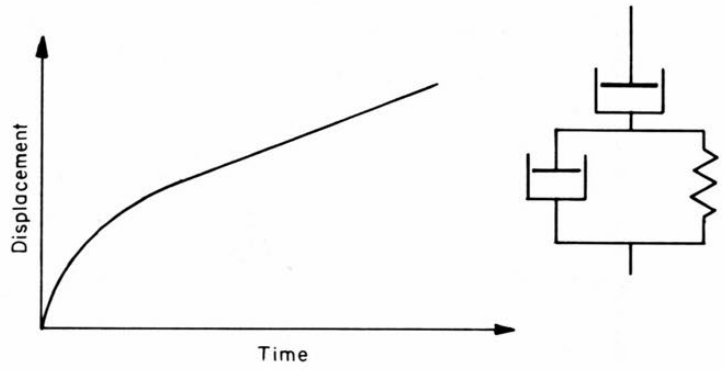

Figure 6. Dashpot-Voigt model.

Mechanical behavior of snow

Cohesive, high-density snow subjected to nondestructive loading behaves as a viscoelastic material.[4 10] The response of snow to such loading can be reasonably well represented by a combination of Maxwell and Voigt rheological models in series. Upon application of a fixed load, there is an instantaneous and recoverable elastic deformation, followed by a decelerating *primary* creep, which is partly recoverable by relaxation, and finally by a steady *secondary* creep, which is not recoverable (Fig. 5). For practical purposes, as shown by Wuori[11] for plate bearing tests, the elastic behavior is quite insignificant and could be neglected. The corresponding rheological model would then consist of a Voigt model in series with a dashpot (Fig. 6). Neither of these models is completely satisfactory since they fail to account for the nonlinear viscosity (plastic behavior) under high stress conditions. At low stresses (considerably below its maximum strength) snow displays linear (Newtonian) viscosity.

The assumption of a purely elastic behavior is likely to be limited to cases where the material is subjected to loads for only short periods of time, no more than a few seconds.[4]

The elastic parameters for snow, such as Young's modulus and Poisson's ratio as a function of density, have been determined experimentally with sufficient reliability [4 12 13] (see Fig. 7 and 8).

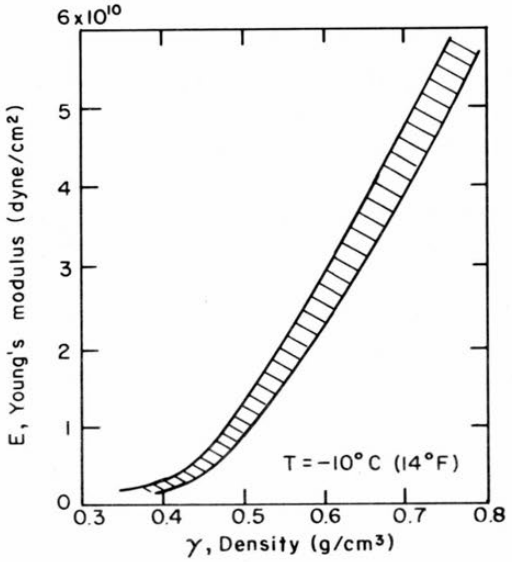

Figure 7. Young's modulus vs density. (After Mellor,[4] Nakaya.[12])

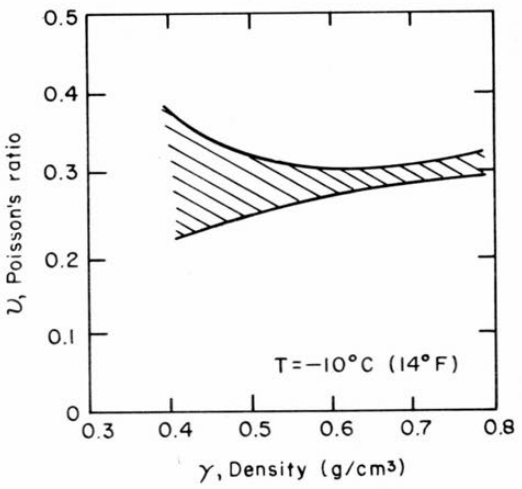

Figure 8. Poisson's ratio vs density. (After Mellor,[4] Smith.[13])

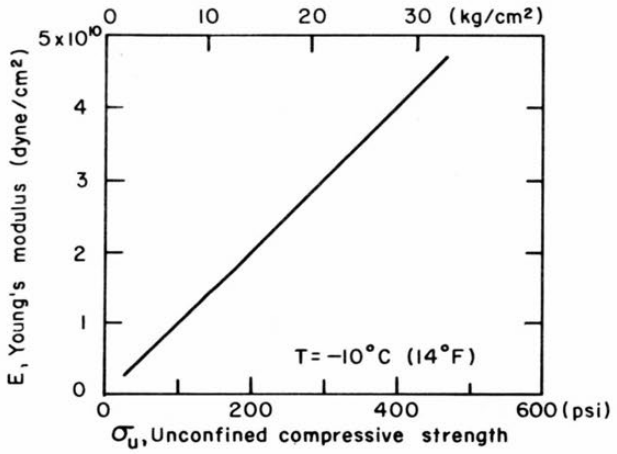

Figure 9. Young's modulus vs unconfined compressive strength. (After Smith.[13])

The relationship between Young's modulus and unconfined compressive strength is shown in Figure 9. (The disagreement between the results of various authors, indicated by the envelopes in Fig. 4, 7, 8, and 9 could be attributed to the various methods of testing.)

Under sustained loading, creep is the principal mechanical process. In snow runway design, this condition would pertain primarily to the aircraft parking areas, but, in most cases, not to the runway itself.

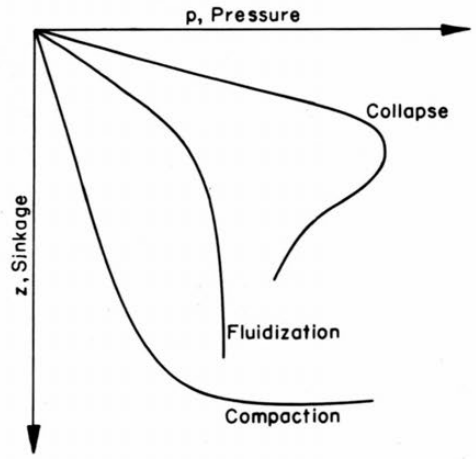

Figure 10. Load-sinkage relations.

Failure mechanism of snow

Under a constant load, gradual consolidation or settlement occurs, which, depending on temperature and density, may lead to ultimate collapse. If loading is sufficiently low, compaction alone may not lead to complete failure of the material, since moderate penetration into snow is usually limited by increasing resistance as the collapsing snow compacts. For moderate loads the phenomenon of progressive failure of bonds and the phenomenon of compaction probably work against each other, producing a linear or quasi-elastic load-sinkage relationship.[14]

Failure in this case is a matter of definition, and in practical applications the definition will vary, depending on the particular application to be considered. Some penetration of a truck wheel on a snow road may not be considered a failure of the pavement if the mobility of the vehicle is not greatly affected. However, the same penetration of an aircraft wheel during a takeoff may result in very serious consequences and, therefore, has to be considered a failure.

Under increasing or repeated loads, progressive deterioration of the material, caused by progressive failure of bonds between particles, will result in a complete loss of cohesion or *fluidization.*

Under sufficiently high stresses, snow fails either by creep rupture or by brittle fracture. If load is applied at a low rate, failure occurs by creep rupture. With increasing loading rate, there is an increase in rupture stress.

The behavior of soils or snow under load, as characterized by pressure-sinkage relations, can be divided into three general classes,[14] as shown in Figure 10. As explained earlier, fluidization, by far the most common case, is caused by progressive breakdown of the material bond structure under increasing load. Compaction usually occurs in high porosity material having weak bonds. A hard crust over a soft foundation will collapse when critical pressure is reached. It is not uncommon for materials to exhibit more than one of the three characteristics. For example, a material can be compacted up to a certain point, but, under continued increasing pressure, ultimately become fluidized.

DESCRIPTION OF EXPERIMENTAL WORK

Method

For this study, a two-dimensional theoretical model could not very well be duplicated in a laboratory experiment. An approximate simulation is possible, however, if the test samples can be made sufficiently thin with respect to their width and height.

Spraying a grid on the face of the snow sample and subjecting the sample to an increasing compressive load permitted the observation of the progressive deformation of the material through a comparison of the deformed grid with a reference grid adjacent to the sample face. The deformation with increasing pressure was recorded by taking photographs at certain intervals during the test. The deformations were then measured from enlarged photographs. A schematic representation of the two-dimensional experimental case is shown in Figure 11.

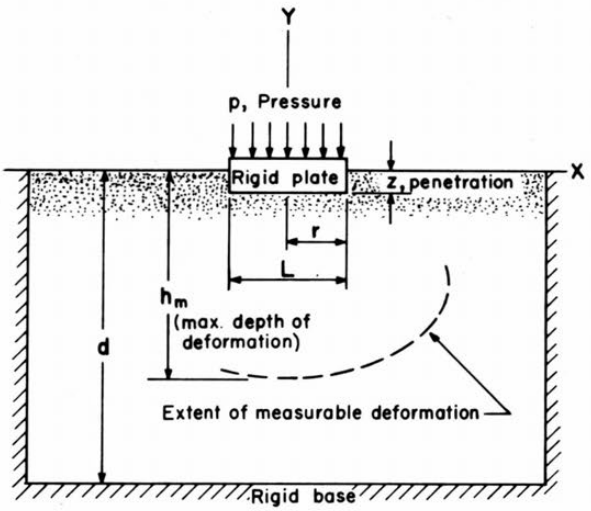

Figure 11. Two-dimensional case.

The following symbols and nomenclature were used:

Symbol	*Description*	*Unit of measurement*
L	width of bearing plate	in.
r	half width of plate (equivalent to radius of a circular plate in the three-dimensional case)	in.
w	length of plate (constant)	in.
p	pressure applied to sample (load/Lw)	psi
z	penetration (sinkage) of plate	in.
s	vertical deformation of sample	in.
h	depth	in.
d	snow sample height	in.
h_m	maximum depth at which measurable deformation occurred	in.
γ	density of snow sample (equivalent to specific gravity)	g/cm^3
σ_u	unconfined compressive strength of sample	psi
σ_i	bearing strength of confined sample (point of initial failure or collapse)	psi

Because of the nature of the available equipment, it was more convenient to obtain the original measurements in the British units, except for density which could be measured more easily in metric units. The experimental data, therefore, are shown in the units originally used in obtaining the data. However, in figures showing generalized interpretations of data or conclusions, both British and metric units are used.

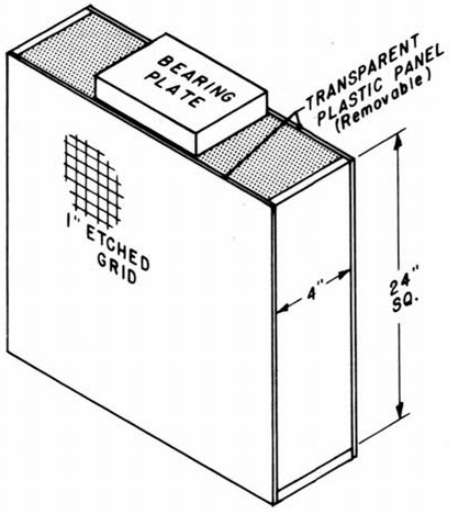

Figure 12. Sample container.

Preparation of test samples

Two types of snow were used: natural and processed (disaggregated with a rotary snowplow). One 4-ft × 2.5-ft × 2.5-ft container was filled with natural snow, which was compacted with a wooden tamper as it was being shoveled into the container. The second container, of the same size, was filled with natural snow without additional compaction. The third container was filled with processed snow directly from the chute of a Klauer rotary snowplow and then dropped on a concrete floor to increase its density. The fourth container was filled with processed snow in the same manner without any attempt to compact it further. Thus, samples of four more or less distinct density ranges were obtained.

These storage containers were immediately transported to the coldrooms, and the snow was allowed to sinter at a constant temperature of –12C (10F) for a period of more than two weeks before testing was begun.

A container to hold the snow samples during the test was constructed as shown in Figure 12.

A slightly oversized sample was sawed off from the large snow block in the storage container. The sides of the sample were then carefully shaved until a perfect fit of the sample into the test container was obtained. For the higher density samples this was quite time consuming. A 1-in. grid was then sprayed on the face of the sample through a carefully cut template, which matched the permanent grid on the transparent front panel. The front panel was then installed, and two U-shaped restraining bars, made of angle iron, were placed vertically around the container to minimize any expansion of the sample during the test. (The plastic panels were not sufficiently rigid to resist expansion of the sample under load.)

A few composite samples, consisting of a layer of processed snow on top of natural snow, were also prepared.

Core samples, 2.7 in. in diameter, for the density measurements and unconfined compressive strength tests, were obtained from the snow block adjacent to the sawed-off sample. The samples were also used for grain size distribution data. The samples were obtained with a core tube having cutting teeth at one end. While the sample was held in a special core holder, its ends were shaved carefully to ensure that they were perpendicular to the vertical axis of the core.

Test apparatus and equipment

A high-capacity mechanical press was used to apply load to the samples at a constant rate of penetration (maximum rate available was 1.5 in./min). A 10,000-lb-capacity proving ring, installed below the upper platen of the press, was utilized to obtain the load data. The same press and proving ring were used for the unconfined compressive strength tests. A dial indicator, calibrated to .0001 in., was used to indicate the bearing plate penetration. The test equipment setup is shown in Figure 13.

Four sizes of bearing plates were used: 4, 6, 8, and 10 in. wide and slightly less than 4 in. long (to allow free movement inside the sample container).

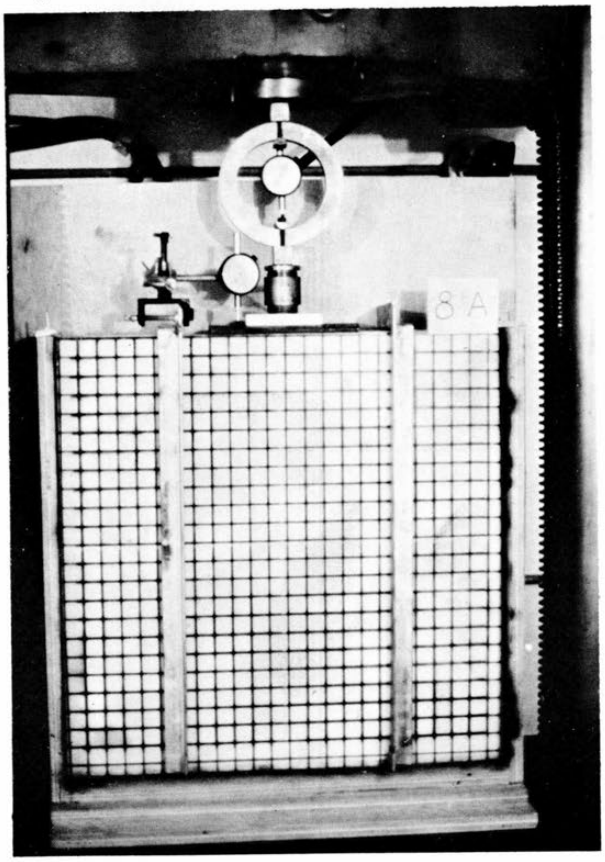

Figure 13. Container with test sample in compression press.

A triple beam balance was used for weighing the core samples; a caliper and an engineer's scale for determining the core dimensions; and a series of U.S. Standard sieves, no. 4, 10, 20, 40, 60, 80, 120, and 200, and a mechanical sieve shaker for determining the particle size distribution.

Procedure

The container with the sample was placed in the press as shown in Figure 13. A reflex Nikon photo camera was mounted on a tripod approximately 3 ft from the face of the sample. To minimize the creep behavior of the sample under load, the load was applied at the maximum available penetration rate of 1.5 in./min.

During the first few tests it was necessary to release the load for a couple of seconds periodically to photograph the deformation and to record the proving ring dial reading and the plate penetration. After a little practice, however, it was possible to perform the test without load release. As the photo camera was operated with the left hand, at the instant the lens shutter was opened, the proving ring reading was observed; and while the reading was being recorded with the right hand, the film in the camera was forwarded with the left hand. By this method the deformation and load data could be obtained every few seconds. It was not possible to record the plate penetration; this information had to be obtained from the photographs.

The test was continued until after failure had occurred; that is, until the apparent maximum strength of the sample was reached before collapse. This was indicated by the dropping off of the proving ring readings. Usually, the point of failure was quite obvious.

A total of 21 tests was performed. The general summary of tests conducted is shown in Table I.

Table I. Summary of tests conducted.

Density (g/cm^3)	*Age* (days)*	*Bearing plate width (in.)*	*Test no.*	*Thickness of processed layer (in.)*
Natural snow				
Not compacted				
0.30	38	10	15	
0.31	38	8	17	
0.34	38	4	16	
Compacted				
0.36	42	8	18	
0.38	31	6	13	
0.38	31	8	14	
Processed				
Not compacted				
0.42	17	4	6	
0.44	25	8	8	
0.44	29	10	12	
0.45	25	6	9	
0.46	17	4	5	
0.47	27	6	10	
Compacted				
0.53	68	8	2	
0.54	68	6	3	
0.56	70	6	7	
0.57	34	4	1	
0.59	70	4	4	
Processed on top of natural snow				
0.52 0.37	85 60	4	21	5
0.52 0.37	85 60	4	23	8
0.54 0.40	75 50	4	19	6
0.54 0.39	75 50	4	20	4

*Time since obtaining sample from the field. For complete data and photographs see Appendixes B and C.

The unconfined compressive strength tests were performed on snow samples 2.7 in. in diameter and between 5.5 and 8 in. long, using the 1.5-in./min constant rate of deformation. Density measurements of the samples were obtained before each test.

Sieve analyses were performed on representative samples from each density range. Two pieces of the sample were rubbed against each other above the top sieve until a 200- to 300-g sample was obtained. Mechanical sieving was done for 2 min, followed by 30 sec of hand sieving of each consecutive sieve.

It is realized that this method does not provide a true picture of the actual grain size distribution in sintered snow. However, assuming that the bonds between the snow grains fail before the grains themselves, some indication of the comparative grain size distribution can be obtained.

RESULTS AND DISCUSSION

Mechanical properties of test samples

The sintering period for virtually all test samples was more than 3 weeks; by then most of the sintering had occurred (see Fig. 2). The age of the snow samples was, therefore, not considered as a variable. The temperature, being a constant during the sintering process and the tests, was also eliminated as a variable. The rate of load application was constant for all tests. Sample size was constant except for a few cases where a smaller sample (18 in. high) had to be used because of apparent structural flaws at one end of the sample.

Therefore, in determining the deformation experimentally, the following parameters were considered:

1. pressure applied	p
2. bearing plate width	L
3. density of sample	γ
4. unconfined compressive strength of sample	σ_u.

The unconfined compressive strength as a function of density of the samples tested is shown in Figure 14. For the density range 0.28 to 0.59 g/cm^3 the relationship can be very nicely represented in the general form

$$\log \sigma_u = a\gamma + b$$

where

σ_u = unconfined compressive strength

γ = density

a, b = constants.

However, this type of relationship has no theoretical basis and does not satisfy the boundary condition $\sigma_u = 0$ at $\gamma = 0$.

Expressing the relationship by log-log plot

$$\sigma_u = b\gamma^a$$

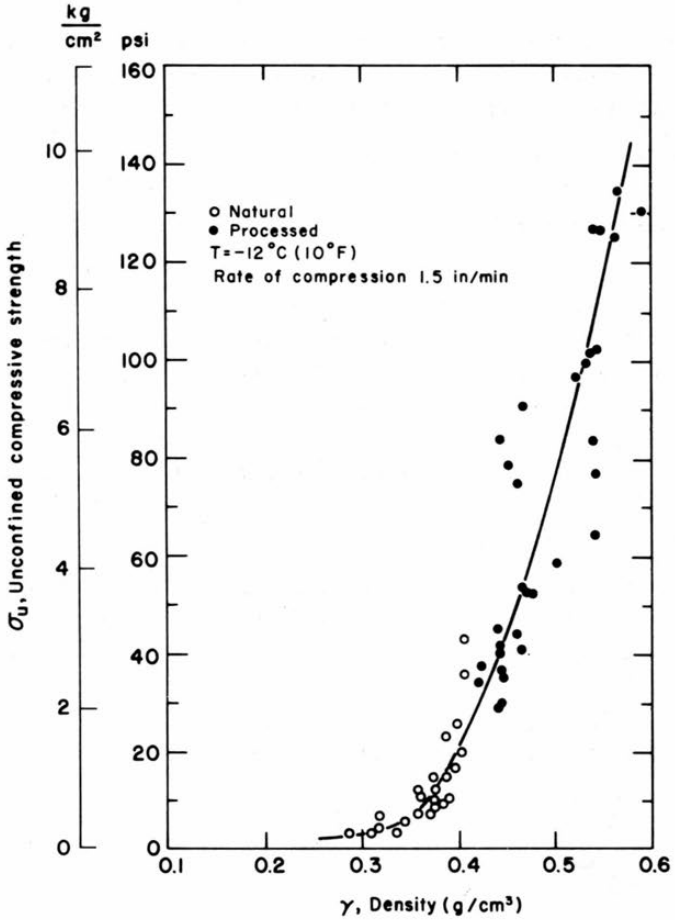

Figure 14. Unconfined compressive strength vs density.

also gives good agreement with data for this density range and satisfies the above boundary condition, but neither this nor any of the several other expressions[15] are applicable for the entire snow density range.

As expected, a strong empirical relationship was observed between the bearing strength of the sample in the container at the initial failure point and its unconfined compressive strength (Fig. 15). It appears that at this particular rate of deformation (1.5 in./min) the unconfined compressive strength of snow is between 70 and 80% of the confined bearing strength. Since the material in the confined state may have some strength while exhibiting no detectable strength in the unconfined state, the intercept may be justified (see Fig. 15).

From a purely theoretical approach, the comparison as shown here does not necessarily represent the difference in strength as such. The material may not fail in the same manner in both the confined and unconfined states; that is, a different failure mechanism may occur in each case. However, for engineering purposes, such as predicting the supporting capacity of a snow runway from unconfined strength data, such a comparison may be quite useful, as long as its limitations (difference in the rate of loading, etc.) are not ignored.

The relative particle size distributions of the natural and processed snows are shown in Figure B1, Appendix B. Although the particle size distribution has an influence on the other mechanical properties of snow,[16] it was not considered as a parameter in this study.

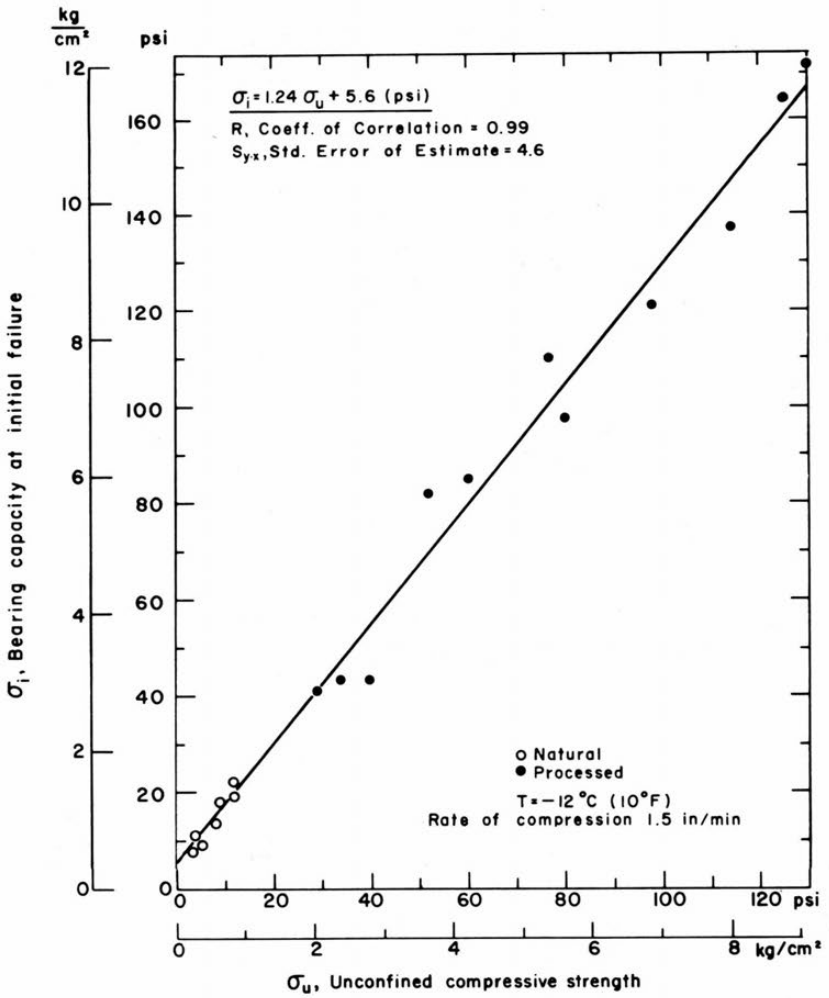

Figure 15. Bearing capacity vs unconfined compressive strength.

Experimental results

Deformation. Since the maximum deformation or displacement at any depth occurred, as expected, directly below the load, the vertical deformations along the y-axis were measured from enlarged photographs (one-half the actual size) and plotted versus depth, as shown in Figure 16. The pressure applied to the snow sample at the time the deformation was photographed is indicated on each deformation curve. The deformation data for samples of similar densities, and thus similar deformation patterns, are plotted on the same graph. The deformation (under center of load) vs depth data for the various snow densities and various pressures are shown in Figures 17 through 23.

It is apparent from these graphs that deformation is a strong function (more so than expected) of the snow density. In low density snow, a high degree of deformation occurred near the surface, the extent of deformation decreasing sharply with depth. In the higher density ($\gamma > 0.45$) samples, the vertical displacement appears to be roughly inversely proportional to depth (Fig. 21 to 23).

The maximum depth at which any measurable vertical deformation occurred (extent of "deformation bulb") appeared to increase with density up to approximately 0.45 (Fig. 17 through 21) and then decrease with an increase in density above 0.5 (Fig. 22, 23). In low density snow, consolidation

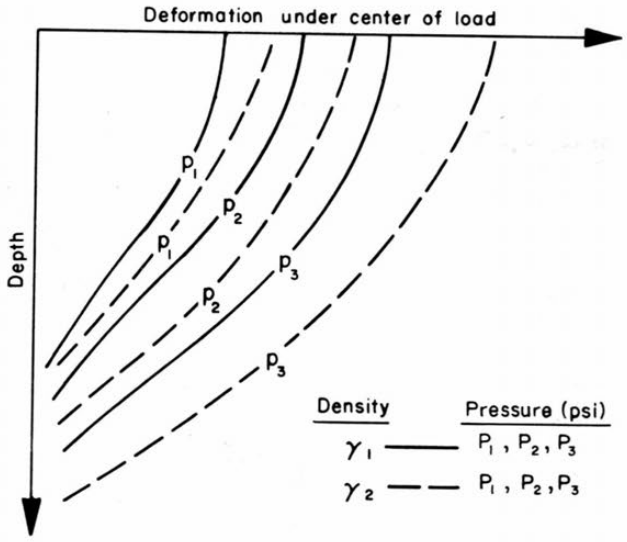

Figure 16. Method used in presenting deformation vs depth data.

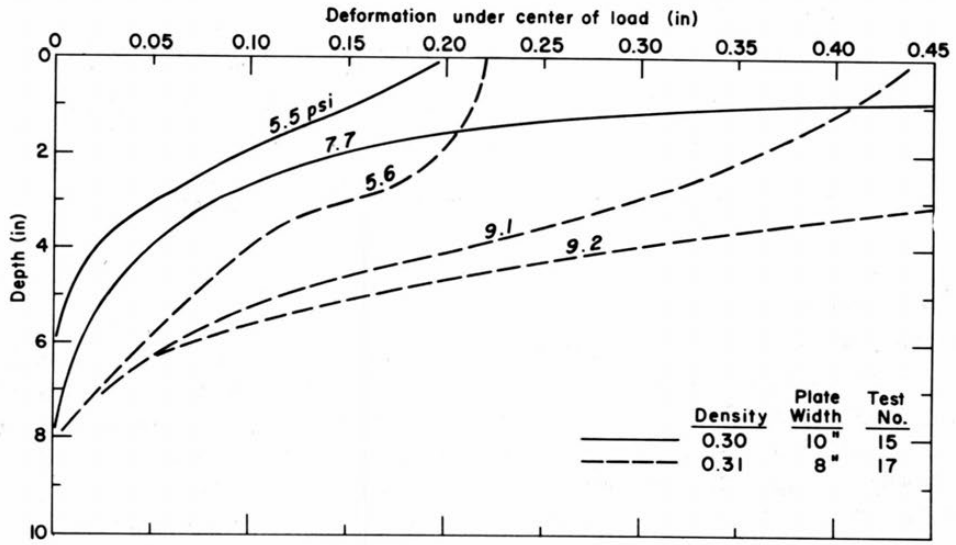

Figure 17. Vertical deformation at Y-axis (density = 0.30-0.31).

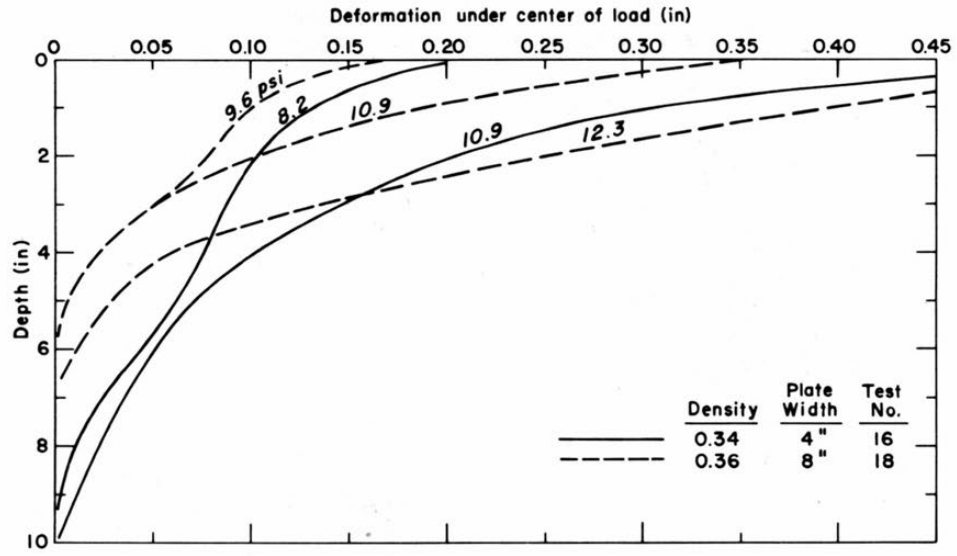

Figure 18. Vertical deformation at Y-axis (density = 0.34-0.36).

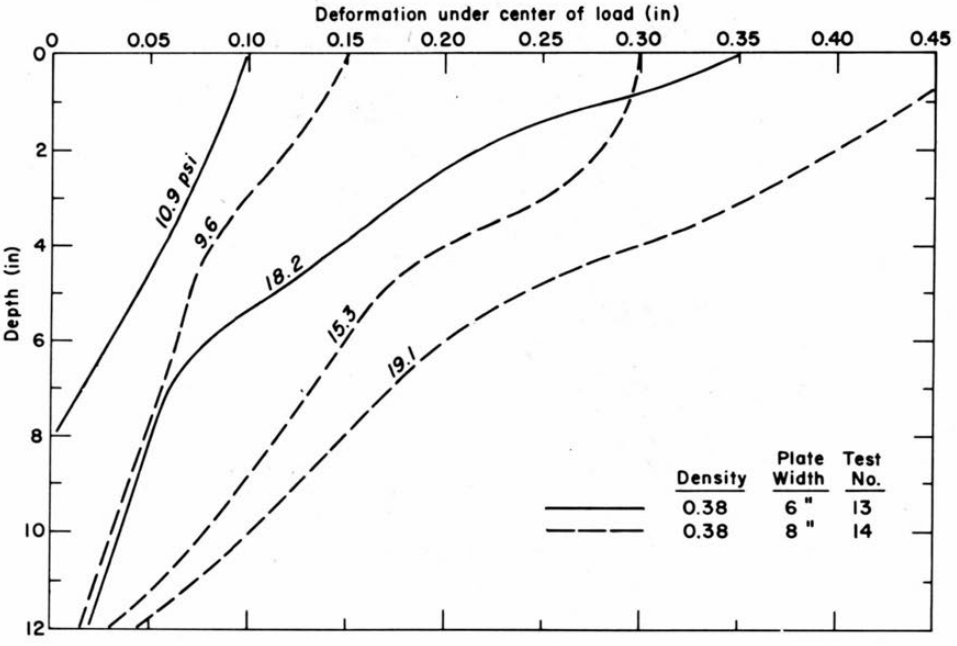

Figure 19. Vertical deformation at Y-axis (density = 0.38).

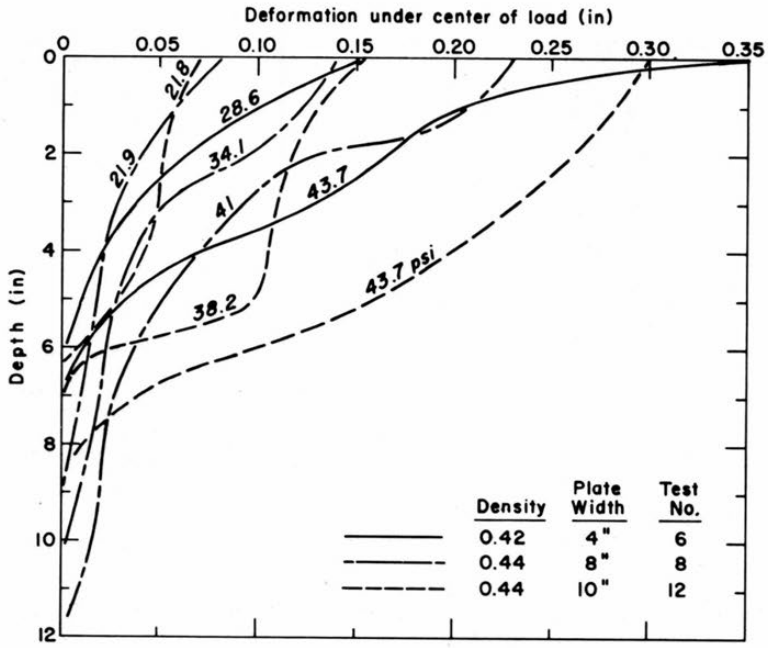

Figure 20. Vertical deformation at Y-axis (density = 0.42-0.44).

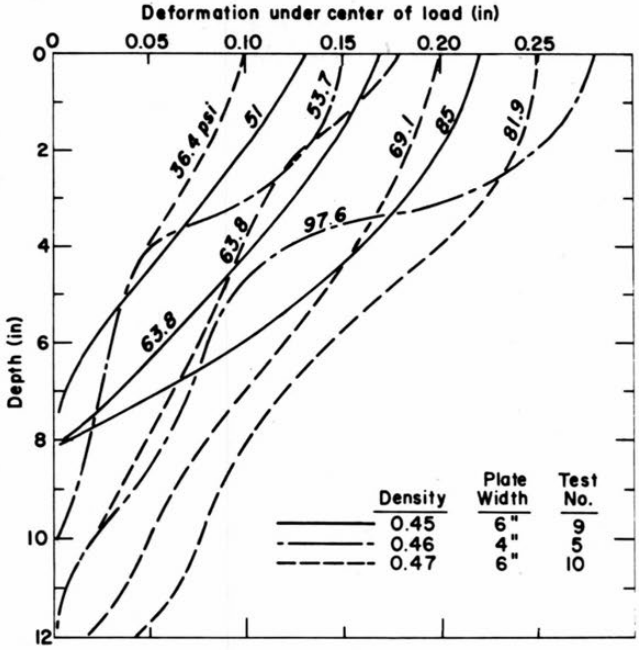

Figure 21. Vertical deformation at Y-axis (density = 0.45-0.47).

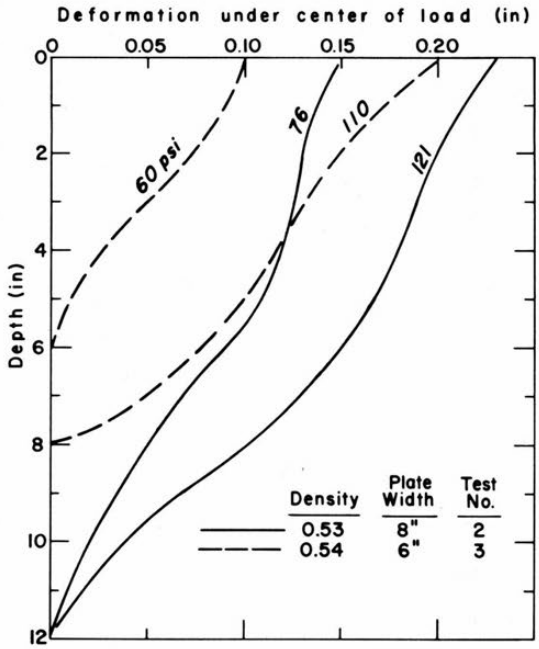

Figure 22. Vertical deformation at Y-axis (density = 0.53-0.54).

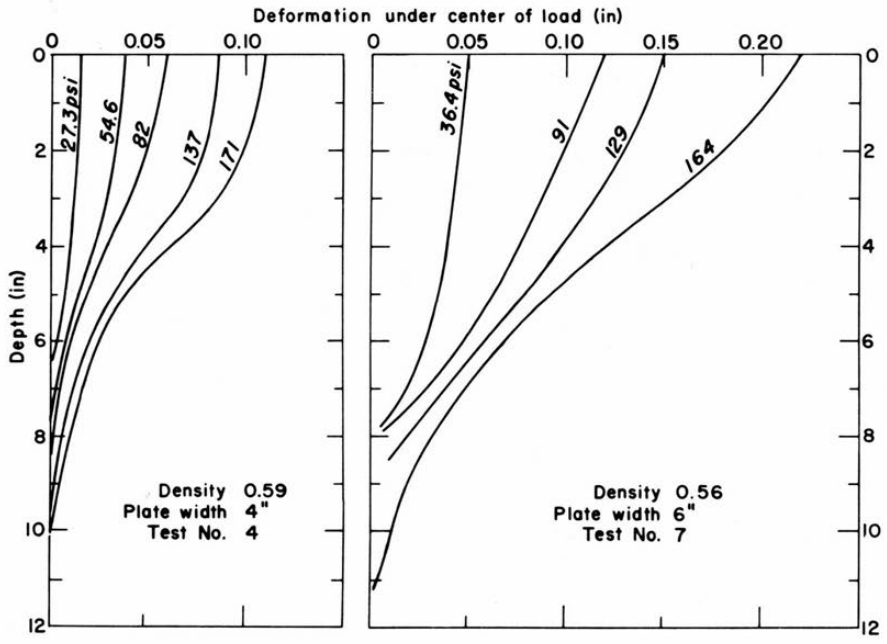

Figure 23. Vertical deformation at Y-axis (density = 0.56; density = 0.59).

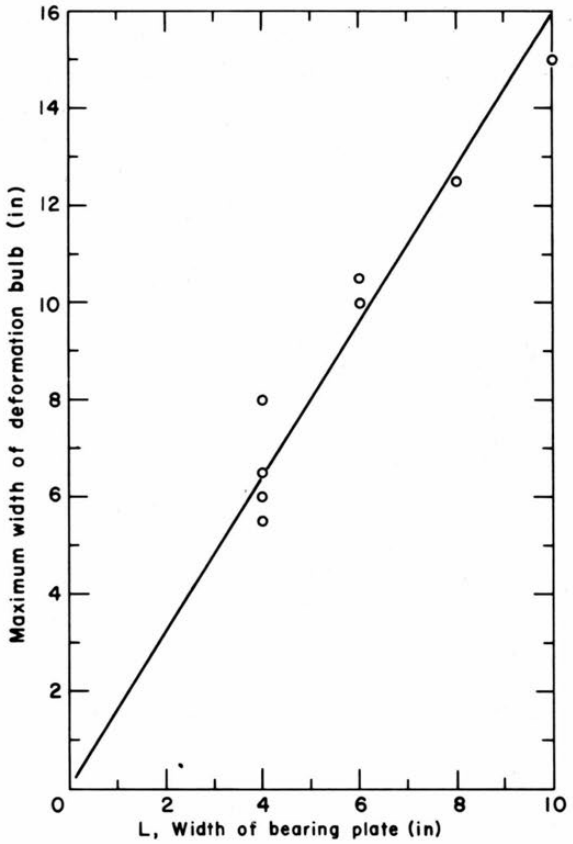

Figure 24. Width of deformation bulb as related to bearing plate size.

of the material because of load occurs near the surface because of the high porosity. As porosity decreases (increase in density), consolidation has to extend deeper to accommodate the displacement of the material from above. At higher densities, collapse or failure occurs at a very low surface deformation, and the small amount of consolidation is apparently absorbed within a relatively short distance from the surface, the ratio of surface deformation/maximum extent of deformation z/h_m approaching a constant. However, the exact depth at which vertical deformation approached zero h_m was difficult to determine.

The data gave no evidence of any apparent relationship between the extent of vertical deformation h_m and the plate width L for the range of plate sizes used (4 to 10 in.). It could be expected that the extent of vertical deformation or displacement would increase with an increase in plate size (all other parameters being constant). To determine the effect of plate size on the extent of vertical displacement (limit of the "deformation bulb"), a more accurate method of measuring deformation and more homogeneous test samples would be required.

The extent of vertical displacement in the horizontal plane (width of the "deformation bulb") could be detected more easily, although it was not obvious in all cases. The apparent maximum width of the "deformation bulb" was approximately 1.6 times the width L of the bearing plate (Fig. 24). This agrees closely with Wuori's[2] figure of 1.5.

The amount of horizontal displacement in all tests was extremely low and could not be measured with any degree of accuracy. This indicates that, as load was applied on top of the snow sample, virtually all consolidation of the material occurred in the vertical direction.

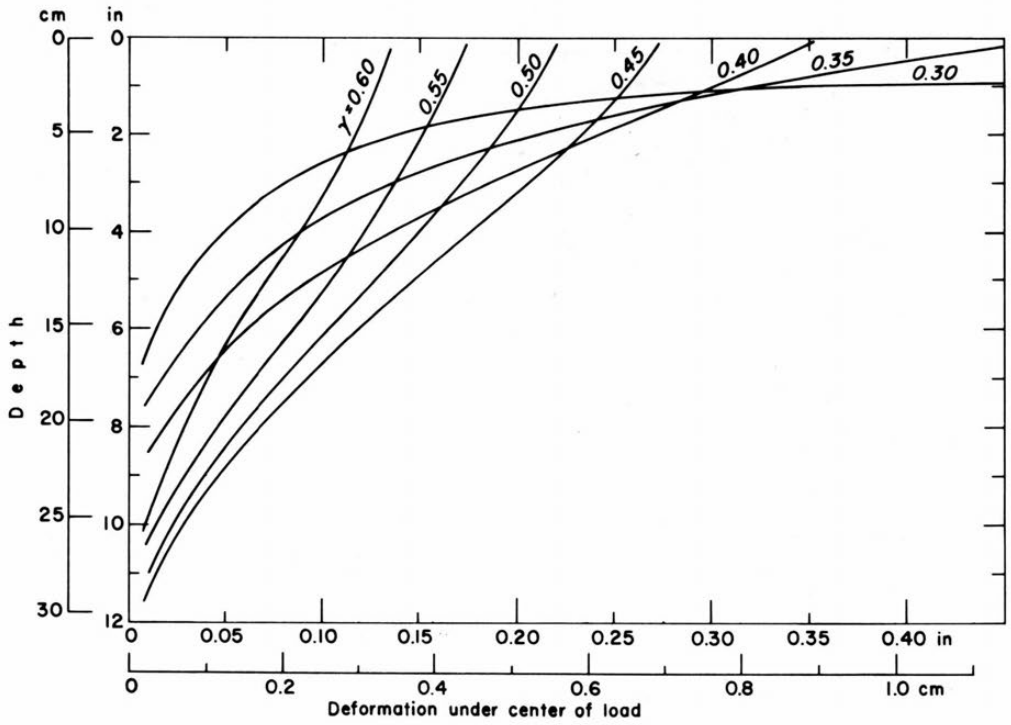

Figure 25. Vertical deformation at initial failure vs depth for various snow densities (generalized representation).

By averaging and interpolating the vertical deformation vs depth data as related to density, a definite pattern can be observed. The generalized relationship between depth and vertical displacement at the point of initial failure as a function of density is shown in Figure 25.

Pressure-sinkage relationships. Plotting the bearing plate penetration as a function of pressure applied (Fig. 26) indicates that penetration up to the initial failure point is a linear function of pressure for snows of density > 0.45.

The apparent change in the behavior of snow at a density of 0.45 is not surprising. Figures 4 and 7 show that 0.45 density is approximately the point below which the relationship between strength (or Young's modulus) and density ceases to be linear.

It is also apparent from Figure 26 that the bearing plate penetration at the failure point ("critical penetration") increases with a decrease in density; that is, in low density snow, the bearing plate penetrates deeper than it does in higher density snow before failure of the material occurs. The "critical penetration" data, as related to density, agree closely with data from Wuori's[11] study of plate penetration into snow (three-dimensional case).

The term *failure*, as used here, does not necessarily represent the ultimate bearing capacity, but indicates the point at which the first significant collapse of the material occurred (initial failure), as explained previously under Procedure, p. 9. The occurrence of this collapse usually could not only be seen but heard.

Since the load was applied at a constant rate of penetration, the deformation (or penetration) scale can also be considered as the time scale, each 0.1-in. increment of penetration being equivalent to 4 sec.

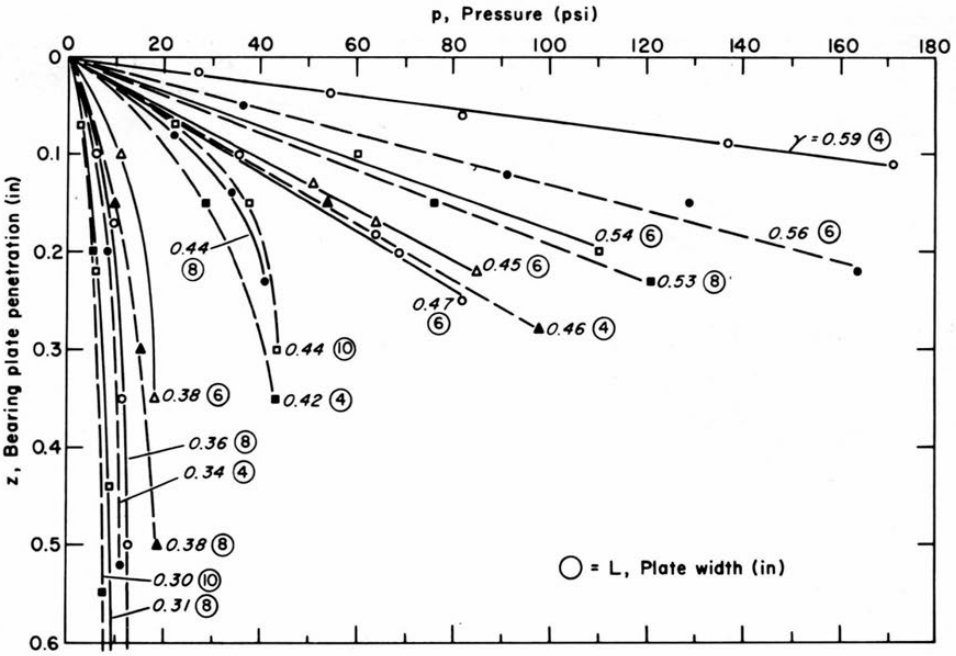

Figure 26. Bearing plate penetration vs pressure.

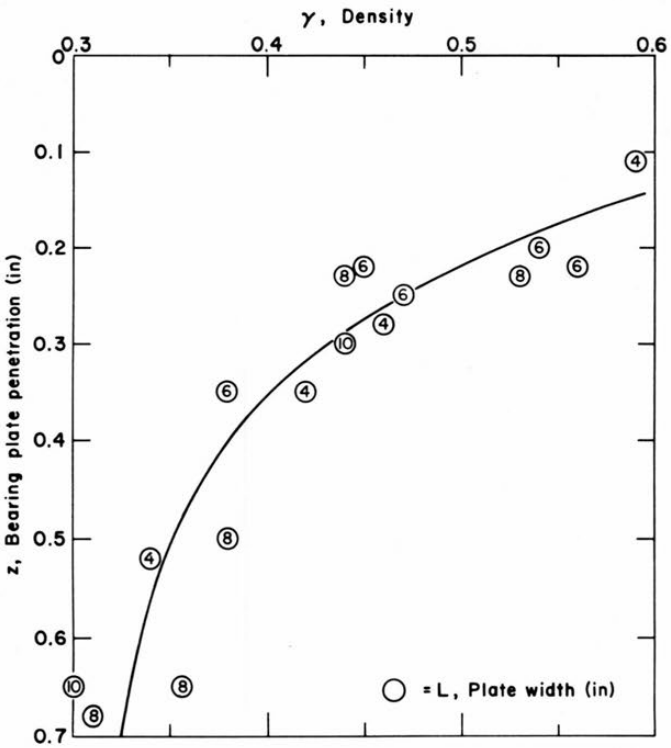

Figure 27. Penetration at initial failure vs density.

The penetration vs pressure data (Fig. 26) give no indication of the effect of plate size (width). The size effect is also not evident if the bearing plate penetration at initial failure ("critical penetration") is plotted vs density (Fig. 27).

Wuori[11] has shown that in the three-dimensional case the penetration of the bearing plate, as well as the deformation of the material, varies measurably with the bearing area. In the simulated two-dimensional case, the bearing area Lw does not increase as rapidly with an increase in L, since w is kept constant. Therefore, in this case a wider range of plate widths might have to be used to observe any trend.

If, however, the data shown in Figure 27 are plotted in a dimensionless plot, such as z/r vs snow density/ice density, the bearing plate size effect becomes more apparent (Fig. 28). By arbitrarily selecting the 4-in. plate as reference and assigning a relative factor, C_r (values shown in Fig. 28) to each of 6-, 8-, and 10-in. plate sizes, good correlation results by plotting z/r vs the density numeric ((density of snow/density of ice)/C_r) as shown in Figure 29. This method of forcing various plate sizes to fit a common curve has been used by Nuttall and McGowan[17] in evaluating pressure-sinkage relationships in snow.

For the density range and plate sizes used, a straight-line relationship results on a log-log plot between density and penetration (z or z/r) at initial failure (Fig. 30). That is, for the density range 0.3 to 0.6, the critical penetration can be related to density by

$$z = a\gamma^{-b}$$

or

$$\frac{z}{r} = a_r\gamma^{-b}$$

where the constant a_r is related to plate size. The amount of data is obviously not sufficient to draw conclusions regarding the size effect from the z/r vs γ plot; however, the general trend is evident.

The dimensionless penetration vs density numeric relationship (Fig. 29) shows no statistical advantage over the z vs γ relationship (Fig. 30) on a log-log plot. The coefficient of correlation for the dimensionless plot is 0.958, while the z vs γ plot gives 0.972.

The data shown in Figure 26 can also be plotted in a quasi-dimensionless form; that is, z/r vs pressure (Fig. 31).

Liston and Hegedus[18] have shown by dimensional analysis that, for a given plate geometry (circular, rectangular), good correlation is obtained by plotting pressure-sinkage data in terms of dimensionless parameters (z/s) vs ($\gamma\ell/p$), where s = plate circumference and ℓ = characteristic length of plate. This method of plotting would not be realistic for the two-dimensional case (or a strip loading in the three-dimensional case), since the circumference s could not be computed. In this case it would be more realistic to plot z/r vs $\gamma\ell/p$. This was tried, but the correlation was very poor. It appeared that the dimensionless parameters do not account properly for the effect of density. Liston and Hegedus[18] used a constant snow density (0.27), and the density of the soil samples varied little. Therefore, the effect of density was not fully investigated. It was also apparent that in the two-dimensional case, these dimensionless parameters do not account properly for the size effect. However, the depth of penetration used by Liston and Hegedus was at least 6 in., while the extent of penetration in this study was confined to less than 1 in.

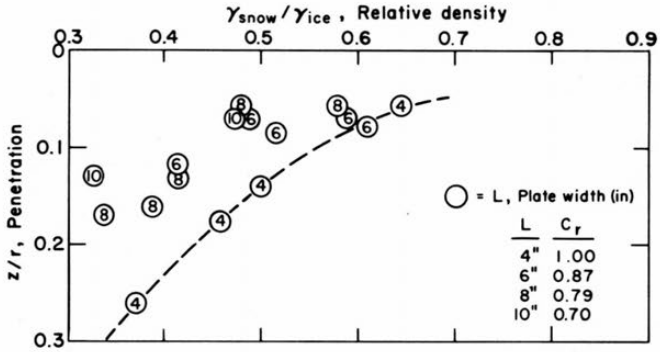

Figure 28. Penetration (z/r) at initial failure vs relative density.

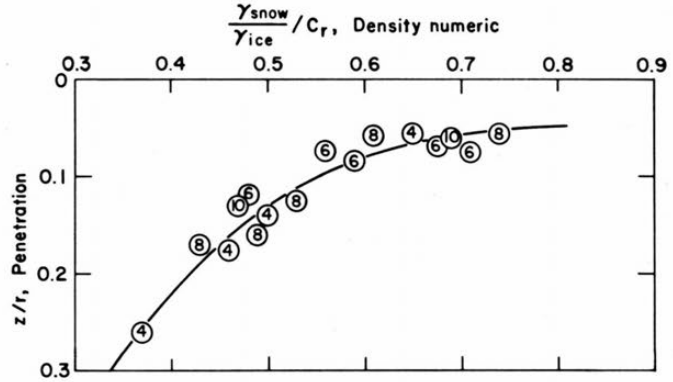

Figure 29. Penetration (z/r) at initial failure vs density numeric.

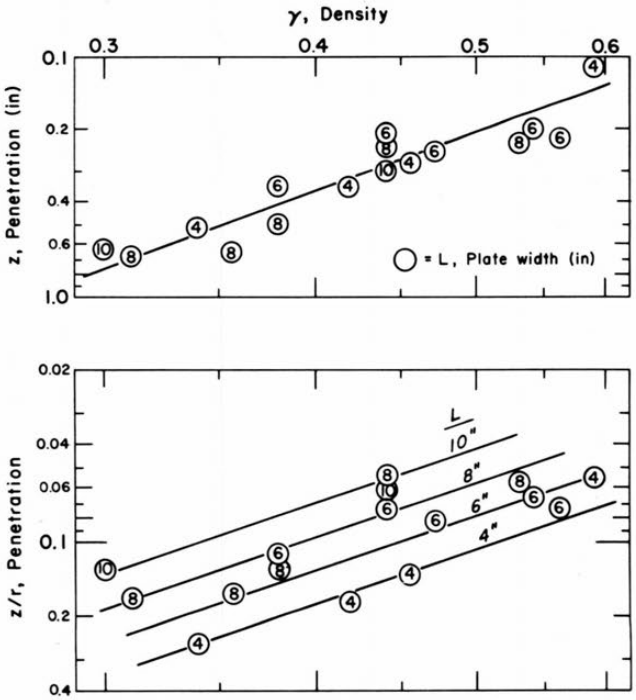

Figure 30. Penetration at initial failure vs density.

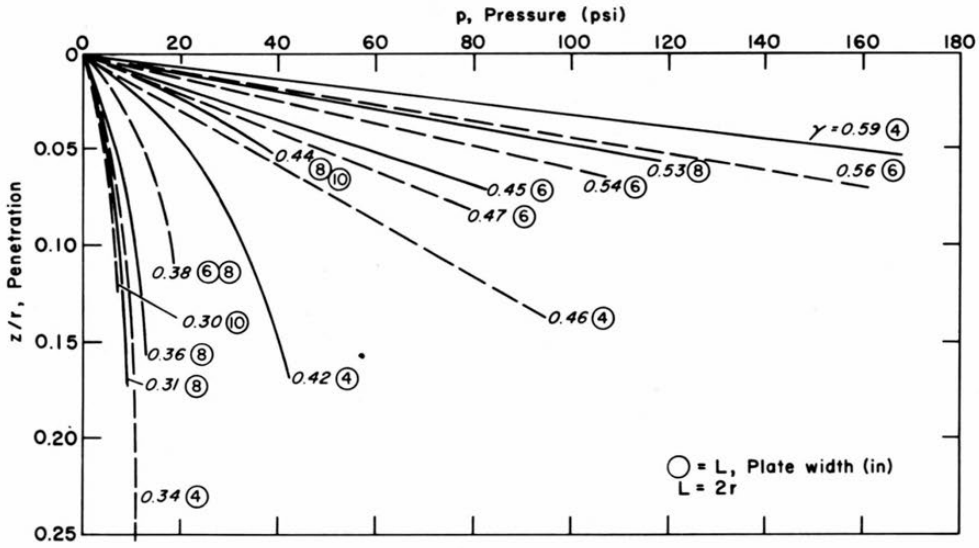

Figure 31. Penetration (z/r) vs pressure.

By averaging and interpolating the pressure-sinkage data shown in Figure 26 and using the density-sinkage relationship shown in Figure 27, a generalized failure envelope can be constructed, which indicates the depth to which a bearing plate will penetrate, or the pressure which can be applied to snow of a particular density before initial failure occurs (Fig. 32). The envelope should vary for different bearing plate sizes, although this was not evident in the z vs p plot for the range of plate sizes used (4 to 10 in. wide). The envelope will also vary for different rates of load application. Temperature will have a strong effect, since the strength of snow varies with temperature.

In the same manner, corresponding initial failure envelopes can be constructed from the z/r vs p data shown in Figure 31. The four-parameter, quasi-dimensionless failure envelopes are shown in Figure 33.

As in the z vs γ log-log plot (Fig. 30), the z vs p relationship at initial failure also yields a straight line on a log-log plot (Fig. 34). The initial failure envelopes from Figure 33 are also shown in a log-log plot in Figure 34.

So far, attention has been given only to the initial failure. In practical applications, the initial failure may not, in some cases, be of great importance. If a wheel penetrates into a snow pavement only a fraction of an inch, causing initial failure, the consequences may not be serious, unless fluidization or ultimate collapse of the material occurs. If further compaction of the material follows the initial failure, the material may be able to support the load for a short period of time, until further collapse, if any, occurs. However, once a complete structural breakdown (fluidization or ultimate collapse) of the material occurs caused by load intensity, repeated loading, or time, the material will not regain load-supporting capacity.

The type of equipment and instrumentation used in the experiments did not permit close observation of the behavior of the snow samples under continued load application after the initial failure or collapse had occurred. However, previous experience and other data, such as from the California Bearing Ratio (CBR) tests[2] and well instrumented unconfined compressive strength tests,[19] give definite indications of the behavior of snow up to the ultimate failure point. For high density snows ($\gamma > 0.45$), the initial collapse is usually followed by a series of repeating collapses, ultimately resulting in a complete breakdown of the material. The z vs p relationship for this case can generally be represented by the fluidization type of curve shown in Figure 10. In reality this is

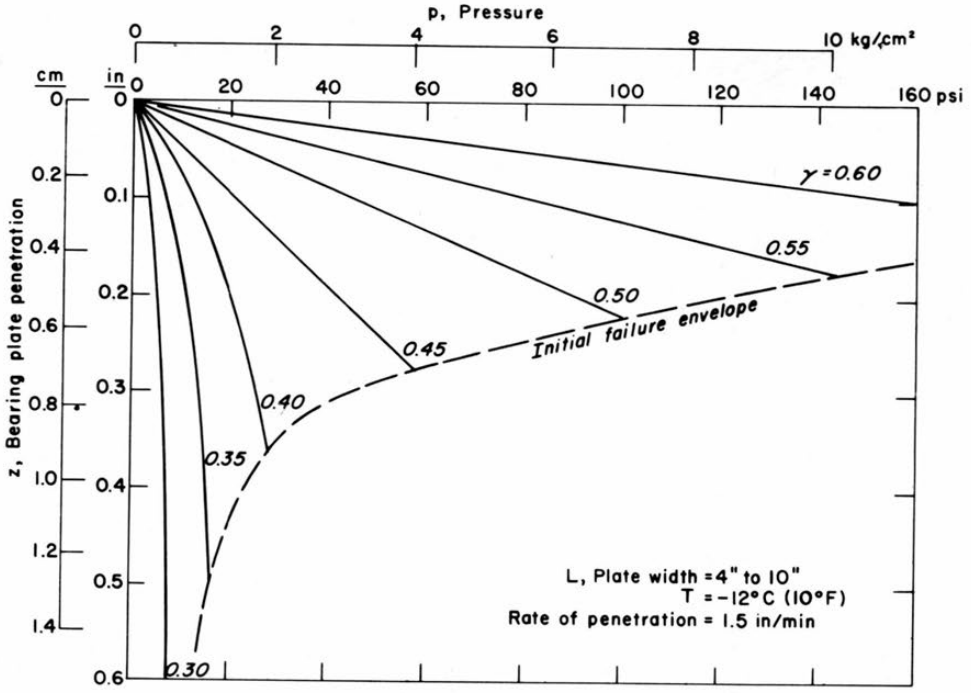

Figure 32. Penetration vs pressure as related to density (generalized representation).

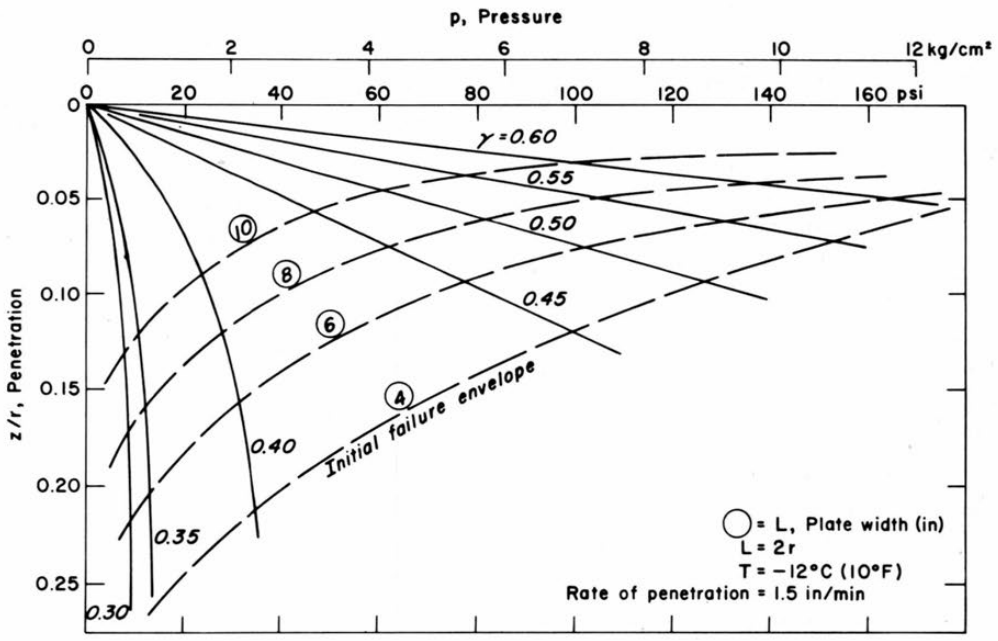

Figure 33. Penetration (z/r) vs pressure as related to density and plate size (generalized representation).

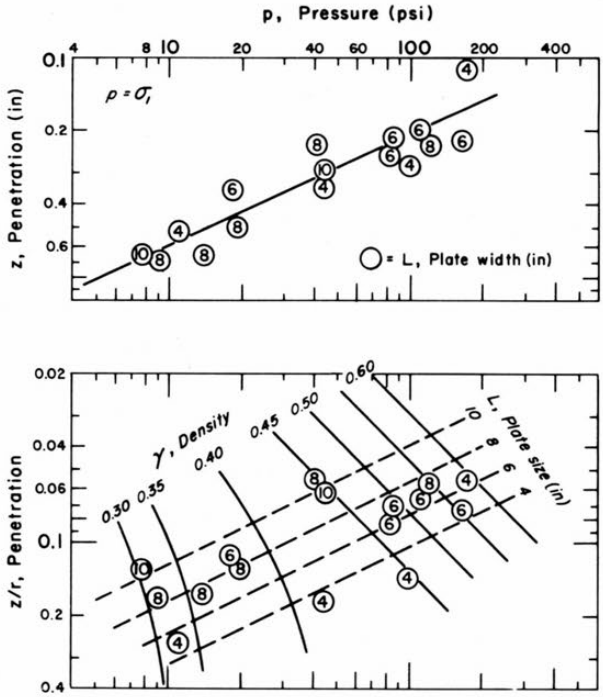

Figure 34. Penetration at initial failure vs pressure.

not a smooth curve, but consists of a series of small collapse and compaction type curves (see Fig. 10); the general shape, however, corresponds to the fluidization curve.

The behavior of low density snow ($\gamma < 0.45$) can generally be represented by the compaction type of curve (see Fig. 10), as far as the general shape of the z vs p relationship is concerned. This curve also consists of a series of small, repeating collapses, each followed by further compaction as shown by Nuttall and McGowan.[17]

A schematic representation of the behavior (progressive failure) of snow under a constant rate of deformation as related to its initial density is shown in Figure 35.

Comparison of experimental data with Assur's pressure-sinkage theory. Assur[14] has shown that the pressure-sinkage relationship for various types of soils and snow can be represented by a common nondimensional curve. This relationship was derived from a rigid theoretical approach. However, very few experimental data were used to verify the theoretical solution, although the data covered a wide range of loads and loading geometries. It was, therefore, of interest to compare the data from this study (the simulated two-dimensional case) with the predicted values.

In the compaction case (see Fig. 10)

$$\frac{z}{p} = \frac{1}{k_1} - \frac{1}{k_1}\beta^2 z^2 \qquad (1)$$

where

$$\beta = \frac{1}{z_m}$$

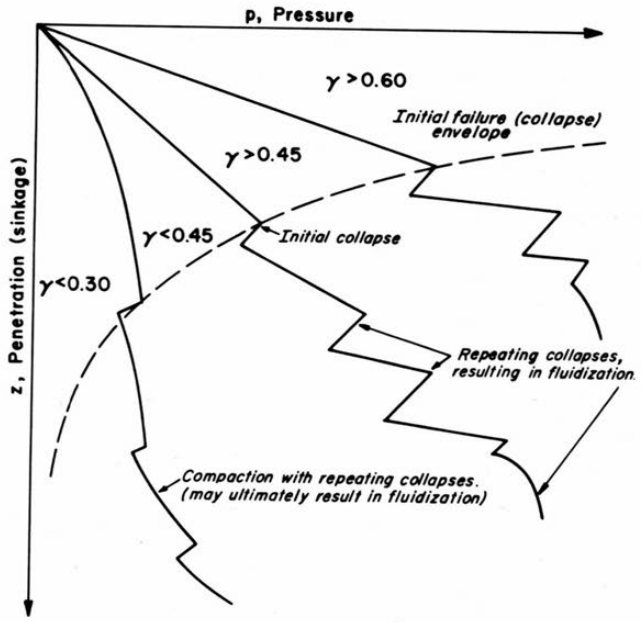

Figure 35. Progressive snow failure.

and in the fluidization case

$$\frac{p}{z} = k_1 - k_1 \alpha^2 p^2 \tag{2}$$

where

$$\alpha = \frac{1}{p_m}.$$

It is first necessary to evaluate the unknown parameters:

k_1 = constant, related to soil or snow "stiffness"

p_m = theoretical maximum bearing capacity

z_m = theoretical maximum sinkage.

By plotting z/p vs z^2, the constant $1/k_1$ is obtained from the intercept in eq 1 at $z = 0$, and z_m can be computed from the negative slope β^2/k_1, where $z_m = 1/\beta$.

The snow data used by Assur represented low density snow, whose z vs p behavior corresponded to the compaction case. In the present study, however, the snow behavior in the density range 0.30 to 0.45 corresponded to the fluidization case. A z/p vs z^2 plot of these data, therefore, yields a positive slope (Fig. 36). While the constant $1/k_1$ can be obtained, z_m does not exist in the fluidization case.

By plotting p/z vs p^2, the constant k_1 can be similarly obtained from the intercept in eq 2 at $p = 0$ and $p_m = 1/\alpha$. This plot of the data is shown in Figure 37.

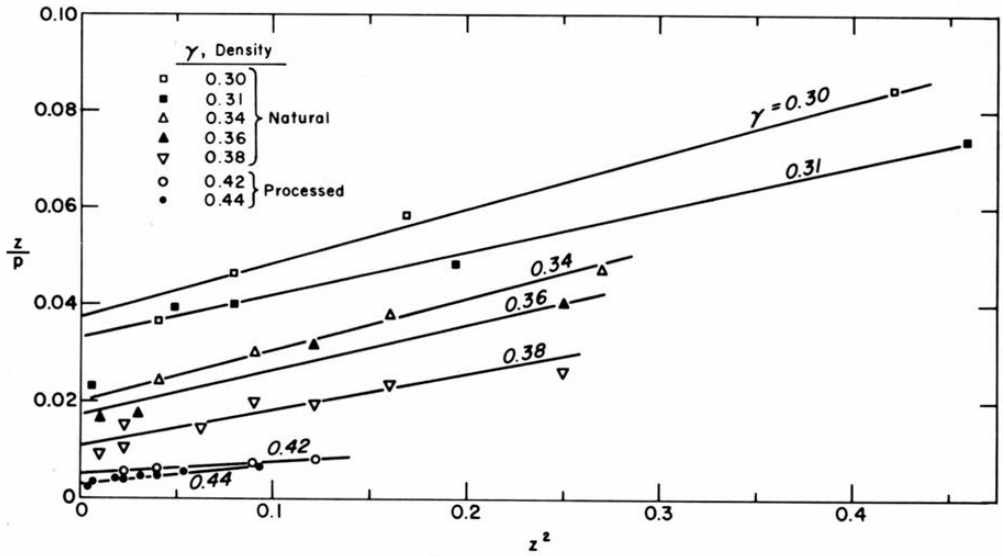

Figure 36. z/p vs z^2.

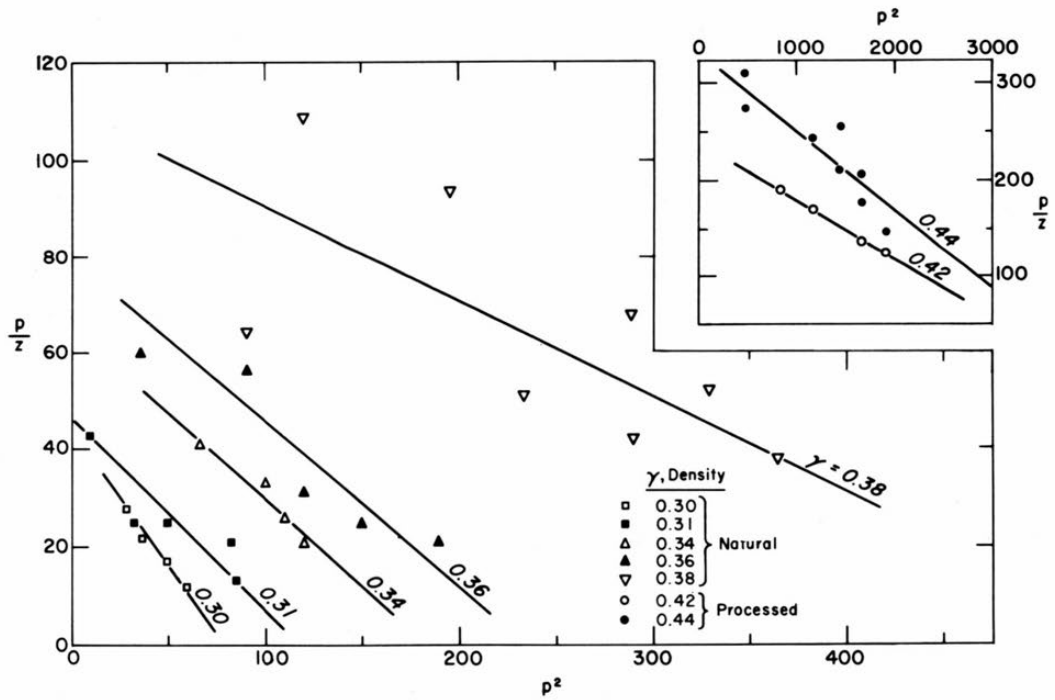

Figure 37. p/z vs p^2.

If the z vs p relation is linear, the slope on either a z/p vs z^2 or a p/z vs p^2 plot will be zero; that is, as long as a material exhibits a linear z vs p relationship, p_m or z_m cannot be predicted. This is the case for snows of density greater than 0.45 before the point of initial failure is reached.

Equation 2, representing the fluidization case, can be rewritten as

$$\frac{k_1 z}{p_m} = \frac{\dfrac{p}{p_m}}{1 - \dfrac{p^2}{{p_m}^2}}. \tag{3}$$

Furthermore, eq 3 can be expressed as

$$\eta = \frac{\chi}{1 - \chi^2} \tag{4}$$

where

$$\eta = \frac{k_1 z}{p_m}$$

$$\chi = \frac{p}{p_m}.$$

Equation 4 represents the unique nondimensional relation[14] which should theoretically accommodate the pressure sinkage behavior of all fluidizing soils and snow after the z vs p relation ceases to be linear.

The k_1 and p_m values were obtained from Figure 37. The values for η and χ were then computed. (The computed values are shown in Table BVII, p. 57.) The data were plotted (Fig. 38) together with Assur's curve. The agreement is quite satisfactory.

It was also of interest to investigate how the parameters k_1 and p_m vary with density. Arithmetical plots yielded exponential curves. To satisfy the condition $k_1 = 0$ and $p_m = 0$ at $\gamma = 0$, the general expressions would, therefore, be in the form

$$k_1 = a\gamma^b$$

and

$$p_m = u\gamma^v$$

where a, b, u, and v are constants.

These relationships are shown in Figure 39. For comparison, the σ_i vs γ relationship is also shown, so that the apparent relationship between the bearing capacity at the initial failure σ_i and the

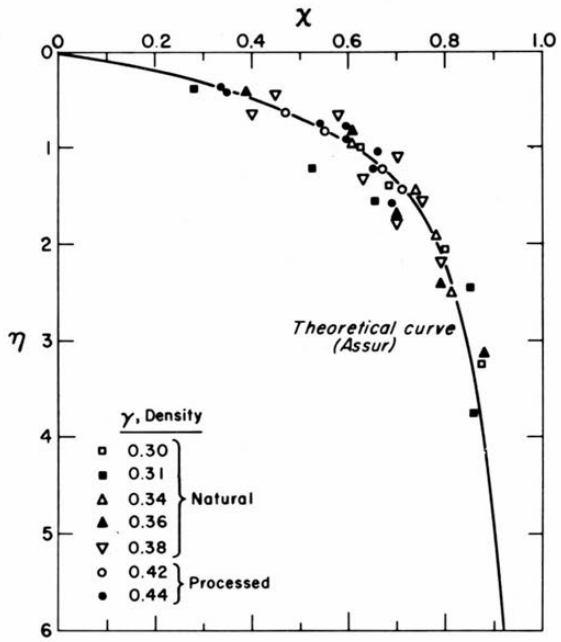

Figure 38. η vs χ, theoretical curve compared with experimental data.

parameters k_1 and p_m can be observed. It is interesting to note that the slopes of all three plots in Figure 39 are almost identical. The small amount of data, however, does not really justify a statistical analysis and comparison of the correlations shown in Figure 39.

Composite samples. Since it was decided to investigate the effect of the thickness of the high density, processed snow mat, the plate size (4 in.) was kept constant, and the selection of the processed and natural snow layers was made so that density would not have to be treated as a variable. Density of mat varied from 0.52 to 9.54 and of the natural snow foundation from 0.37 to 0.40. Four different mat thicknesses were used: 4, 5, 6, and 8 in.

The plate penetration vs pressure plot (Fig. 40) shows that initial failure, in this case a true collapse, occurred at virtually the same plate penetration regardless of the mat thickness. This observation, from only four tests, should not lead to a conclusion. It would be reasonable to expect that an increase in mat thickness would allow more penetration (surface deformation of the mat) before collapse occurs. The range of mat thickness used is not really sufficient to determine the thickness effect on the bearing capacity, although the trend is evident (Fig. 41).

It was earlier determined that the bearing capacity σ_i of snow in the density range 0.37 to 0.40 was between 20 and 30 psi (see Fig. 32 and 33). This would represent the bearing capacity of the foundation; that is, mat thickness = 0. Similarly, the bearing capacity of 0.52 to 0.54 density snow was between 120 and 150 psi for the 18- or 24-in.-deep samples. This information allows a logical extrapolation of the mat thickness vs σ_i relationship indicated by the four data points in Figure 41.

The manner in which the mat was supported on the foundation does not simulate exactly a full-scale situation. In the experiment the mat width (24 in.) could not really be considered infinite, as in the case of a runway pavement. The ends of the mat were not fixed. Neither can this case be related to a long narrow beam resting on a weak foundation. And, of course, different mat density/foundation density ratios will yield different results. In general, the failure of the mat was caused by consolidation of the weaker foundation below, and the mat failed in flexure.

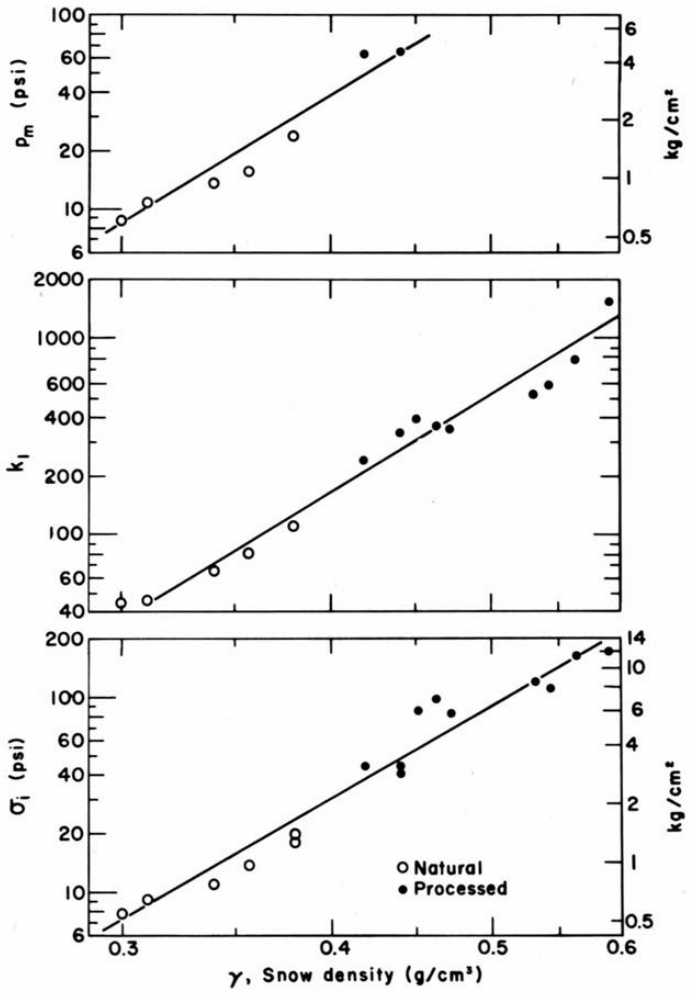

Figure 39. σ_i, k_1, and p_m vs density.

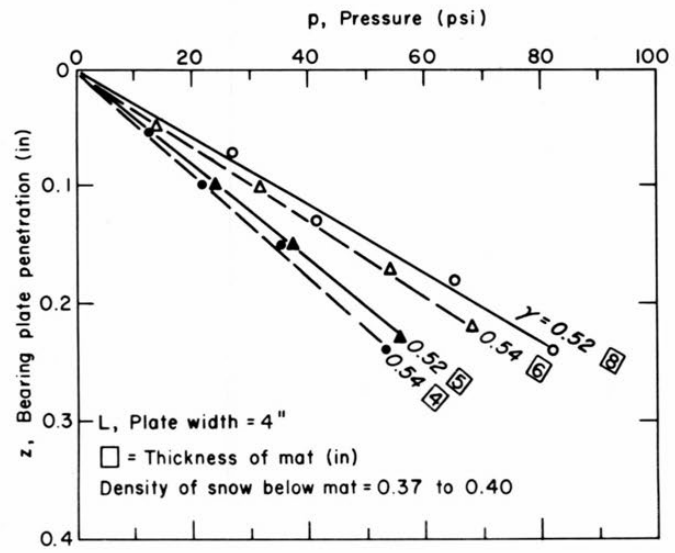

Figure 40. Penetration vs pressure (composite samples).

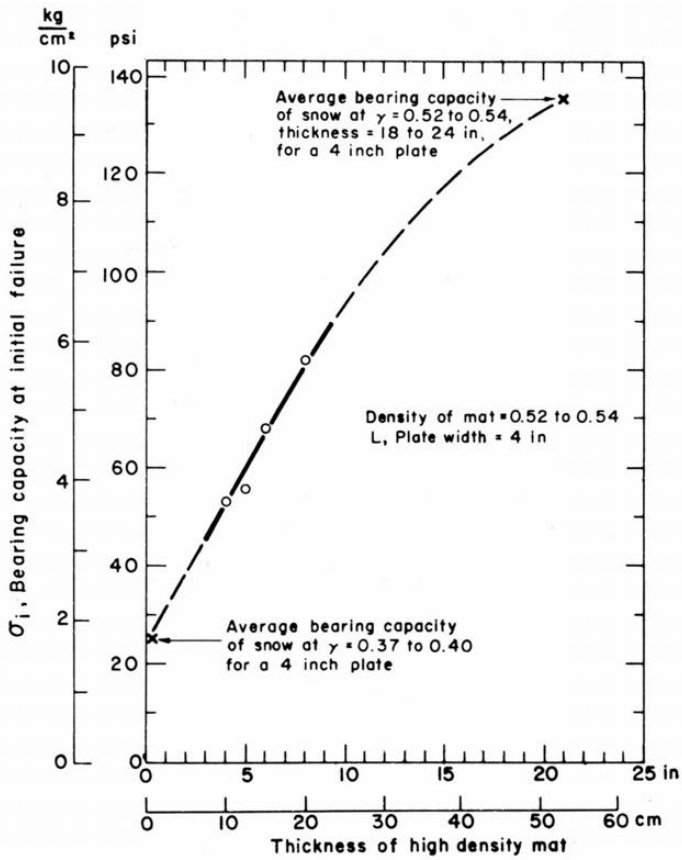

Figure 41. Bearing capacity vs mat thickness.

SUMMARY, CONCLUSIONS, AND RECOMMENDATIONS

In actual field practice, the density of snow is not a very reliable parameter for estimating strength or bearing capacity of a snow pavement. However, if the effects of other parameters, such as temperature, age of snow or sintering time, and rate of loading are minimized, density can be used as a very convenient index for predicting the behavior of snow under a load.

In this study the following parameters were considered as variables: bearing plate size, pressure applied, and snow density (all strength parameters being considered as functions of density). Bearing capacity, sinkage of bearing plate, and deformation of the material with depth were considered the dependent variables as related to density, pressure, and plate size.

The relationship between penetration (sinkage) and pressure as a function of density, the deformation with depth, and the extent of deformation under a load in a simulated two-dimensional case were determined from experimental data.

For snow of density between 0.45 and 0.6 g/cm^3, the sinkage was a linear function of pressure up to the point of initial failure (bearing strength in a confined state). For snow of density between 0.3 and 0.45, the relationship was nonlinear, the rate of penetration increasing with an increase in pressure (see Fig. 32).

Sinkage at the point of initial failure (critical penetration) decreased with an increase in density; that is, failure in high density snow occurred at a lower bearing plate penetration than in low density snow (see Fig. 27 and 32).

In the density range 0.3 to 0.6 g/cm^3, the sinkage at the failure point could be conveniently represented as a power function of density (see Fig. 30):

$$z = a\gamma^{-b}.$$

Similarly, the bearing strength could be expressed as a power function of density (see Fig. 39):

$$\sigma_i = m\gamma^n.$$

Neither of the above expressions may be valid for the entire snow density range; however, in the 0.3 to 0.6 density range the correlations were quite satisfactory, the coefficients of correlation being greater than 0.9.

The critical penetration data from this study agreed closely with the critical penetration data from Wuori's[11] study of plate penetration into snow, representing the three-dimensional case.

For the range of plate sizes used (4 to 10 in.), no conclusive evidence of the effect of plate size on the bearing strength of snow could be observed. The size effect was not evident unless penetration was plotted nondimensionally as a ratio of penetration/plate size (see Fig. 30 and 34).

The generalized relationship between sinkage and pressure as a function of density and plate size, up to the point of failure, could be represented as shown in Figure 33.

The density of snow had a pronounced influence on the deformation below the load. In low density snow ($\gamma < 0.45$), most of the deformation (consolidation) occurred near the surface, the amount of vertical deformation decreasing sharply with depth. In higher density snow ($\gamma > 0.45$), the vertical deformation was approximately inversely proportional to depth.

The generalized relationship between depth and the deformation under the center of load at the failure point, as related to density, could be represented as shown in Figure 25.

The area of deformation in the vertical plane (deformation bulb) was similar in shape to the typical Boussinesq stress bulb. The apparent width of the deformation bulb was approximately 1.6 times the width of the bearing plate. However, the effect of the plate size on the apparent depth of the deformation bulb was not evident for the range of plate sizes used.

The amount of horizontal displacement below the load was negligible, indicating that virtually all consolidation occurred in the vertical direction.

The experimental pressure-sinkage data showed very good agreement with the theoretical relationship developed by Assur[14] (see Fig. 38). It also appeared that in snow the material constants k_1 and p_m could be related to density (see Fig. 39).

The data from composite samples (high density mat on low density foundation) were limited; however, the effect of mat thickness on the bearing strength of the sample was quite evident (see Fig. 41).

The attempt to develop satisfactory deformation and stress distribution expressions from a theoretical approach was not successful (see Appendix A).

In recent years a very useful optical method for measuring deformation of a body or material, the Moiré fringe method,[20 21 22 23] has been developed to a point where its application may possibly be extended to materials such as snow. This method enables very clear visual observations of the manner and extent of deformation, as in the photoelastic methods used in strain analysis in steel

and other materials. The degree of success in using the Moire' fringe method for measuring deformations in snow (or soils) depends primarily on the ability to spray a fine, accurate grid system on the material. It would be extremely desirable to investigate the possible applications of this method to the study of snow and soil deformation under loads.

LITERATURE CITED

1. Abele, G.; Ramseier, R.O. and Wuori, A.F. (1966) Design criteria for snow runways. *The Engineering Journal* (May), p. 23. Also USA CRREL TR 212, 1968, AD 681220.
2. Wuori, A.F. (1962) Supporting capacity of processed snow runways. U.S. Army Cold Regions Research and Engineering Laboratory (USA CRREL) Technical Report 82, p. 5-16, AD 287049.
3. Bader, H.; Haefeli, R.; Bucher, E.; Neher, J.; Eckel, O. and Thams, Chr. (1954) Snow and its metamorphism. U.S. Army Snow Ice and Permafrost Research Establishment (USA SIPRE) Translation 14, p. 8.
4. Mellor, M. (1966) Snow mechanics. *Applied Mechanics Reviews*, vol. 19, no. 5, p. 380-381.
5. Fuchs, A. (1960) Structure of age-hardening disaggregated Peter snow. USA SIPRE Research Report 53, p. 3-10.
6. Ramseier, R.O. and Sander, G.W. (1966) Temperature dependence and mechanism of sintering. USA CRREL Research Report 189, p. 4-6, AD 640150.
7. Wuori, A.F. (1963) Snow stabilization for roads and runways. USA CRREL Technical Report 83, p. 9, AD 414995.
8. Bender, J. (1956) Testing of a compacted snow runway (U). USA SIPRE Technical Report 42 (Confidential).
9. Paige, R.A. (1965) Strength properties of processed snow. U.S. Naval Civil Engineering Laboratory, Technical Note, p. 12-13.
10. Nevel, D.E. (1965) Creep of a semi-infinite snow mass under external loads. USA CRREL Technical Note (unpublished), p. 4-5.
11. Wuori, A.F. (1957) Plate bearing tests on compacted snow surfaces. Michigan Technological University, Master's Thesis, p. 35-58.
12. Nakaya, U. (1959) Visco-elastic properties of snow and ice in the Greenland Ice Cap. USA SIPRE Research Report 46, p. 8-16.
13. Smith, J.L. (1965) The elastic constants, strength, and density of Greenland snow as determined from measurements of sonic wave velocity. USA CRREL Technical Report 167, p. 4-9, AD 632357.
14. Assur, A. (1964) Locomotion over soft soil and snow. Paper presented at The Automotive Engineering Congress, Detroit, Michigan, 13-17 January, p. 2-6.
15. Kovacs, A. (1967) Density, temperature and the unconfined compressive strength of polar snow. USA CRREL Special Report 115, p. 13-15, AD 660309.
16. Waterhouse, R.W. (1964) On the mechanical stability of snow. USA CRREL Technical Note (unpublished), p. 2-3.
17. Nuttall, C.J. and McGowan, R.P. (1961) Scale models of vehicles in soils and snows. *Proceedings of the 1st International Conference on the Mechanics of Soil-Vehicle Systems* (Torino, Italy), p. 661-662.
18. Liston, R.A. and Hegedus, E. (1964) Dimensional analysis of load sinkage relationships in soils and snows. U.S. Army Tank and Automotive Command Technical Report 8692, p. 17-45.

LITERATURE CITED (Cont'd)

19. Abele, G. (1964) Snow as a construction material. Paper presented at The New England District Meeting of American Society of Civil Engineers, American Society for Testing Materials, National Society of Professional Engineers, University of New Hampshire, April, p. 7.

20. Guild, J. (1956) *The interference systems of crossed diffraction gratings.* Oxford: Clarendon Press.

21. Post, D. (1965) The Moiré grid-analyzer, method for strain analysis. *Experimental Mechanics,* Nov.

22. Theocaris, P.S. (1962) Moiré fringes: a powerful measuring device. *Applied Mechanics,* May.

23. Weller, R. and Shepard, B.M. (1948) Displacement measurement by mechanical interferometry. *Proceedings, Society for Experimental Stress Analysis,* vol. VI-1, p. 35-38.

24. Sneddon, I.N. (1951) *Fourier transforms.* New York: McGraw-Hill Book Co., Inc., p. 411.

25. Timoshenko, S. and Goodier, J. (1951) *Theory of elasticity.* New York: McGraw-Hill Book Co., Inc.

26. Orr, C. and Dalla Valle, J.M. (1960) *Fine particle measurement.* New York: MacMillan Co., p. 29-35.

SELECTED BIBLIOGRAPHY

Abele, G. (1963) A correlation of unconfined compressive strength and ram hardness of processed snow. U.S. Army Cold Regions Research and Engineering Laboratory (USA CRREL) Technical Report 85, AD 299263.

_____ (1963) Trafficability in snow trenches. USA CRREL Technical Report 88, AD 430193.

_____ (1964) Snow as a construction material. Paper presented at the New England District Meeting of American Society of Civil Engineers, American Society for Testing Materials, and National Society of Professional Engineers, University of New Hampshire, April.

_____ (1964) Construction of a snow runway at Camp Century for wheel landings with lightweight aircraft. USA CRREL Special Report 62, AD 609981.

_____ (1965) Subsurface transportation methods in deep snow. USA CRREL Technical Report 160, AD 631949.

_____ and Frankenstein, G. (1967) Snow and ice properties as related to roads and runways in Antarctica. USA CRREL Technical Report 176, AD 665386.

Abele, G.; Ramseier, R.O. and Wuori, A.F. (1966) Design criteria for snow runways. *The Engineering Journal,* May. Also USA CRREL Technical Report 212, 1968, AD 681220.

Arctic Construction and Frost Effects Laboratory (ACFEL) (1954) Project Mint Julep, Investigation of a smooth ice area of the Greenland Ice Cap, Part IV. Report of Arctic Construction and Frost Effects Laboratory, U.S. Army Engineer Division, New England, ACFEL Technical Report 50.

Assur, A. (1964) Locomotion over soft soil and snow. Paper presented at the Automotive Engineering Congress, Detroit, Michigan, Jan.

Bader, H.; Haefeli, R.; Bucher, E.; Neher, J.; Eckel, O. and Thams, Chr. (1954) Snow and its metamorphism. USA SIPRE Translation 14.

Ballard, G.E.H. and Feldt, E.D. (1965) Considerations of the strength of snow. USA CRREL Research Report 184, AD 631000.

Ballard, G.E.H. and McGaw, R.W. (1965) A theory of snow failure. USA CRREL Research Report 137, AD XL624198.

Bender, J. (1956) Testing of a compacted snow runway (U). USA SIPRE Technical Report 42.

Biot, M.A. (1941) Consolidation settlement under a rectangular load distribution. *Journal of Applied Physics,* vol. 12, May.

Butkovich, T.R. (1962) Studies of the age hardening of processed snow. USA CRREL Research Report 99, AD 284939.

Douglas, R.A. (1963) *Introduction to solid mechanics.* Belmont, Calif.: Wadsworth Publication Co.

Feldt, E.D. and Ballard, G.E.H. (1965) An approach to the consolidation of snow. USA CRREL Research Report 181, AD 630648.

Frost Effects Laboratory, U.S. Army Engineer Division, New England (1947) Report of Corps of Engineers observers on Project Snowman. ACFEL Technical Report 15.

_____ (1949) Investigation of snow compaction methods conducted for Engineer Research and Development Laboratories. ACFEL Technical Report 22, with Appendix.

Fuchs, A. (1960) Structure of age-hardening disaggregated Peter snow. USA SIPRE Research Report 53.

SELECTED BIBLIOGRAPHY (Cont'd)

Gow, A.J. (1965) Snow studies in Antarctica. USA CRREL Research Report 177, AD 631718.

_____ and Ramseier, R.O. (1964) Age hardening of snow at the South Pole. USA CRREL Research Report 112, AD 614430.

Guild, J. (1956) *The interference systems of crossed diffraction gratings.* Oxford: Clarendon Press.

Hough, B.K. (1959) Compressibility as the basis for soil bearing value. *Journal of the Soil Mechanics and Foundations Division,* American Society of Civil Engineers, vol. 85, no. SM4, Aug.

Ishihara, K. (1962) General theory of stresses and displacements in two-layer viscoelastic systems. *Soil and Foundation,* vol. 2, no. 2.

Kovacs, A. (1967) Density, temperature and the unconfined compressive strength of polar snow. USA CRREL Special Report 115, AD 660309.

Lee, E.H. (1955) Stress analysis in viscoelastic bodies. *Quarterly of Applied Mathematics,* vol. 13.

Lee, T.M. (1963) Method of determining dynamic properties of viscoelastic solids employing forced vibrations. USA CRREL Research Report 122, AD 434085.

Liston, R.A. and Hegedus, E. (1964) Dimensional analysis of load sinkage relationships in soils and snows. U.S. Army Tank and Automotive Command Technical Report 8692.

Mellor, M. (1966) Snow mechanics. *Applied Mechanics Reviews,* vol. 19, no. 5.

_____ and Hendrickson, G. (1965) Confined creep tests in polar snow. USA CRREL Research Report 138, AD 613043.

Mellor, M. and Ramseier, R.O. (1965) Penetration of plates in viscoelastic snow. USA CRREL Research Report 151, AD 617617.

Mellor, M. and Smith, J.H. (1966) Strength measurements in snow. USA CRREL Research Report 168, AD 631717.

Moser, E.H. (1963) Navy cold processing - Snow compaction techniques. In *Ice and Snow.* Cambridge, Mass.: MIT Press.

Nakaya, U. (1959) Visco-elastic properties of snow and ice in the Greenland Ice Cap. USA SIPRE Research Report 46.

_____ (1959) Visco-elastic properties of processed snow. USA SIPRE Research Report 58.

_____ (1961) Elastic properties of processed snow with reference to its internal structure. USA CRREL Research Report 82, AD 277541.

Nevel, D.E. (1965) Creep of a semi-infinite snow mass under external loads. USA CRREL Technical Note (unpublished).

Nuttall, C.J. and McGowan, R.P. (1961) Scale models of vehicles in soils and snows. *Proceedings of the 1st International Conference on the Mechanics of Soil-Vehicle Systems,* Torino, Italy.

Orr, C. and Dalla Valle, J.M. (1960) *Fine particle measurement.* New York: MacMillan Co.

Ostle, B. (1963) *Statistics in research.* Ames, Iowa: The Iowa State University Press.

Paige, R.A. (1965) Strength properties of processed snow. U.S. Naval Civil Engineering Laboratory, Technical Note.

Pipes, L.A. (1946) *Applied mathematics for engineers and physicists.* New York: McGraw-Hill, Inc.

Post, D. (1965) The Moiré grid-analyzer, method for strain analysis. *Experimental Mechanics,* Nov.

SELECTED BIBLIOGRAPHY (Cont'd)

Ramseier, R.O. (1966) Some physical and mechanical properties of polar snow. USA CRREL Research Report 116, AD 631685.

_____ and Keeler, C.M. (1967) The sintering process in snow. USA CRREL Research Report 226, AD 651452.

Ramseier, R.O. and Sander, G.W. (1966) Temperature dependence and mechanism of sintering. USA CRREL Research Report 189, AD 640150.

Selig, E.T. and McKee, K.E. (1961) Static and dynamic behavior of small footings. *Journal of the Soil Mechanics and Foundations Division,* American Society of Civil Engineers, vol. 87, no. SM6, Dec.

Smith, J.L. (1965) The elastic constants, strength, and density of Greenland snow as determined from measurements of sonic wave velocity. USA CRREL Technical Report 167, AD 632357.

Sneddon, I.N. (1951) *Fourier transforms.* New York: McGraw-Hill Book Co., Inc.

Spangler, M.G. (1951) *Soil engineering.* Scranton: International Textbook Co.

Taylor, A.E. (1955) *Advanced calculus.* New York: Ginn and Co.

Taylor, D.W. (1948) *Fundamentals of soil mechanics.* New York: John Wiley & Sons, Inc.

Theocaris, P.S. (1962) Moiré fringes: A powerful measuring device. *Applied Mechanics,* May.

Timoshenko, S. and Goodier, J.N. (1951) *Theory of elasticity.* New York: McGraw-Hill, Inc.

Waterhouse, R.W. (1964) On the mechanical stability of snow. USA CRREL Technical Note (unpublished).

Weller, R. and Shepard, B.M. (1948) Displacement measurement by mechanical interferometry. *Society for Experimental Stress Analysis Proceedings,* vol. VI-I.

Wuori, A.F. (1957) Plate bearing tests on compacted snow surfaces. Michigan Technological University, Master's Thesis.

_____ (1962) Supporting capacity of processed snow runways. USA CRREL Technical Report 82, AD 287049.

_____ (1963) Snow stabilization for roads and runways. USA CRREL Technical Report 83, AD 414995.

_____ (1963) Snow stabilization studies. In *Ice and Snow.* Cambridge, Mass.: MIT Press.

Yosida, Z. (1956) Physical studies on deposited snow. In *Contributions from the Institute of Low Temperature Science.* Hokkaido University, Sapporo, Japan.

APPENDIX A. DEVELOPMENT OF THEORETICAL EQUATIONS

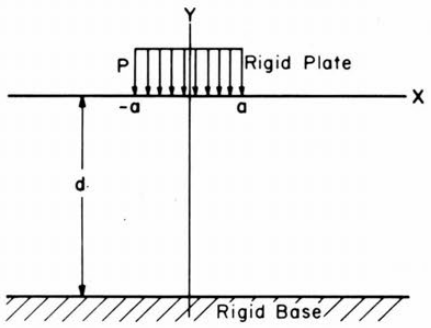

Figure A1.

General considerations

A rigid theoretical treatment for a nonlinear viscoelastic continuum is extremely difficult. It is, therefore, necessary to concentrate on the dominant rheological characteristics of the material for each problem under consideration.

For a practical problem, such as the behavior of a high-strength snow pavement under a concentrated load for a short period of time, the assumption of linear viscosity may be justified. Another assumption that can be made is that the snow is homogeneous and isotropic. This, however, is not quite true in the real case.

Nevel[10] has shown how Boussinesq's solution for external loads on a semi-infinite continuum might be modified for a linear viscoelastic material.

In the case of a snow runway on the Greenland or the Antarctic ice cap, the material could usually be considered to be of infinite depth. In some cases, however, the snow mass of some thickness may rest on ice or some earth material. In any laboratory experiment, the sample would naturally have to be finite. Therefore, the theoretical investigation was limited to the case where the material is of finite depth.

General solution (elastic case)

The problem under consideration is shown in Figure A1. The development of the solution is shown below.

Stress components:

Normal: σ_x, σ_y

Shear: τ_{xy}

Displacement components:

Horizontal: u

Vertical: v

Strain components:

$$\epsilon_x = \frac{\partial u}{\partial x} \tag{A1}$$

$$\epsilon_y = \frac{\partial v}{\partial y} \tag{A2}$$

$$\gamma_{xy} = \frac{\partial u}{\partial y} + \frac{\partial v}{\partial x} \tag{A3}$$

from which can be derived the condition of compatibility

$$\frac{\partial^2 \epsilon_x}{\partial y^2} + \frac{\partial^2 \epsilon_y}{\partial x^2} = \frac{\partial^2 \gamma_{xy}}{\partial x \partial y}.$$

Neglecting body forces, the equations of equilibrium are

$$\frac{\partial \sigma_x}{\partial x} + \frac{\partial \tau_{xy}}{\partial y} = 0 \tag{A4}$$

$$\frac{\partial \sigma_y}{\partial y} + \frac{\partial \tau_{xy}}{\partial x} = 0. \tag{A5}$$

The compatibility equation in terms of stress components can be expressed as

$$\left(\frac{\partial^2}{\partial x^2} + \frac{\partial^2}{\partial y^2}\right)\left(\sigma_x + \sigma_y\right) = 0. \tag{A6}$$

The stress-strain relationships can be expressed as

$$\frac{E}{1 + \nu} \epsilon_x = (1 - \nu)\, \sigma_x - \nu \sigma_y \tag{A7}$$

$$\frac{E}{1 + \nu} \epsilon_y = (1 - \nu)\, \sigma_y - \nu \sigma_x \tag{A8}$$

$$\frac{E}{2(1 + \nu)} \gamma_{xy} = \tau_{xy} \tag{A9}$$

where:

E = Young's modulus

ν = Poisson's ratio.

By taking any function ϕ of x and y, eq A4 and A5 are satisfied by

$$\sigma_x = \frac{\partial^2 \phi}{\partial y^2} \tag{A10}$$

$$\sigma_y = \frac{\partial^2 \phi}{\partial x^2} \tag{A11}$$

$$\tau_{xy} = -\frac{\partial^2 \phi}{\partial x \partial y}. \tag{A12}$$

Substituting expressions A10, A11 and A12 into eq A6, it is found that the stress function ϕ must satisfy the equation

$$\frac{\partial^4 \phi}{\partial x^4} + 2 \frac{\partial^4 \phi}{\partial x^2 \partial y^2} + \frac{\partial^4 \phi}{\partial y^4} = 0. \tag{A13}$$

The function ϕ then satisfies the two-dimensional biharmonic equation

$$\nabla^4 \phi = 0.$$

By using the Fourier transform of the stress function, defined here as

$$\overline{\phi} = \int_{-\infty}^{\infty} \phi(x,y)\, e^{i\omega x}\, dx \tag{A14}$$

and the inverse of the stress function as

$$\phi = \int_{-\infty}^{\infty} \overline{\phi}\,(\omega, y)\, e^{-i\omega x}\, d\omega \tag{A15}$$

the transformation of eq A13 can be performed as follows:

$$\text{Transform of } \frac{\partial^4 \phi}{\partial x^4} = (-i\omega)^4\, \overline{\phi} \tag{A16}$$

$$\text{Transform of } \frac{\partial^4 \phi}{\partial y^4} = \frac{d^4 \overline{\phi}}{dy^4} \tag{A17}$$

$$\text{Transform of } \frac{2\partial^4 \phi}{\partial x^2 \partial y^2} = 2(-i\omega)^2 \frac{d^2 \overline{\phi}}{dy^2}. \tag{A18}$$

Therefore,

$$\frac{d^4\bar{\phi}}{dy^4} - 2\omega^2\frac{d^2\bar{\phi}}{dy^2} + \omega^4\bar{\phi} = 0. \tag{A19}$$

Solving for $\bar{\phi}$ by using the Laplace transform, defined here as

$$L(\bar{\phi}) = \int_{-\infty}^{\infty} \bar{\phi}(\omega,y)\, e^{-sy}\, dy$$

the following general expression is obtained

$$\bar{\phi} = (A_1 + B_1\omega y)\, e^{-\omega y} + (C_1 + D_1\omega y)\, e^{\omega y} \tag{A20}$$

where the arbitrary constants A_1, B_1, C_1 and D_1, which may be functions of ω, are determined from the boundary conditions imposed in the particular problem.

Similarly, the strain and stress components, eq A1, A3, A10, A11 and A12, can be transformed as follows:

$$\bar{\epsilon}_x = (-i\omega)\bar{u} \tag{A21}$$

$$\bar{\gamma}_{xy} = \frac{\partial\bar{u}}{\partial y} - (i\omega)\bar{v} \tag{A22}$$

$$\bar{\sigma}_x = \frac{\partial^2\bar{\phi}}{\partial y^2} \tag{A23}$$

$$\bar{\sigma}_y = (-i\omega)^2\bar{\phi} = -\omega^2\bar{\phi} \tag{A24}$$

$$\bar{\tau}_{xy} = (i\omega)\frac{\partial\bar{\phi}}{\partial y}. \tag{A25}$$

Substituting the appropriate expressions above into the transform eq A7 and A9, the transform displacement equations are obtained:

$$\frac{E}{1+\nu}(-i\omega)\bar{u} = (1-\nu)\frac{\partial^2\bar{\phi}}{\partial y^2} + \nu\omega^2\bar{\phi} \tag{A26}$$

and

$$\bar{\gamma}_{xy} = \frac{\partial\bar{u}}{\partial y} - (i\omega)\bar{v} = \frac{2(1+\nu)}{E}(i\omega)\frac{\partial\bar{\phi}}{\partial y}$$

which yields

$$\frac{E}{1+\nu}\omega^2\bar{v} = (1-\nu)\frac{\partial^3\bar{\phi}}{\partial y^3} + (\nu-2)\omega^2\frac{\partial\bar{\phi}}{\partial y}. \tag{A27}$$

Differentiating eq A20 yields

$$\frac{\partial\bar{\phi}}{\partial y} = \omega(-A_1 - B_1\omega y + B_1)e^{-\omega y} + \omega(C_1 + D_1\omega y + D_1)e^{\omega y} \tag{A28}$$

$$\frac{\partial^2\bar{\phi}}{\partial y^2} = \omega^2(A_1 + B_1\omega y - 2B_1)e^{-\omega y} + \omega^2(C_1 + D_1\omega y + 2D_1)e^{\omega y} \tag{A29}$$

$$\frac{\partial^3\bar{\phi}}{\partial y^3} = \omega^3(-A_1 - B_1\omega y + 3B_1)e^{-\omega y} + \omega^3(C_1 + D_1\omega y + 3D_1)e^{\omega y}. \tag{A30}$$

By proper substitution, eq A23 through A27 can be rewritten as follows

$$\bar{\sigma}_x = \omega^2\{[A_1 + B_1(\omega y - 2)]e^{-\omega y} + [C_1 + D_1(\omega y + 2)]e^{\omega y}\} \tag{A31}$$

$$\bar{\sigma}_y = -\omega^2[(A_1 + B_1\omega y)e^{-\omega y} + (C_1 + D_1\omega y)e^{\omega y}] \tag{A32}$$

$$\bar{\tau}_{xy} = i\omega^2\{[-A_1 - B_1(\omega y - 1)]e^{-\omega y} + [C_1 + D_1(\omega y + 1)]e^{\omega y}\} \tag{A33}$$

$$\bar{u} = -\frac{(1+\nu)}{Ei}\omega\left[\left\{A_1 + B_1[\omega y - 2(1-\nu)]\right\}e^{-\omega y} + \left\{C_1 + D_1[\omega y + 2(1-\nu)]\right\}e^{\omega y}\right] \tag{A34}$$

$$\bar{v} = \frac{(1+\nu)}{E}\omega\left[\left\{A_1 + B_1[\omega y + (1-2\nu)]\right\}e^{-\omega y} - \left\{C_1 + D_1[\omega y - (1-2\nu)]\right\}e^{\omega y}\right]. \tag{A35}$$

Boundary conditions. Assuming that the stress distribution directly below the load is not known, it can be designated with some function $q(x)$. The load condition, however, is symmetrical; therefore, it can be stated that $q(x)$ is an even function.

It can further be stated that the rigid foundation below the material at depth d does not permit vertical deformation v to occur at $y = d$, and that the foundation is a rough surface, so that friction will not permit horizontal deformation u to occur at $y = d$.

Therefore,

$$\sigma_y = q(x) = \left.\begin{array}{ll} -q(x) & (x < a) \\ 0 & (x > a) \end{array}\right| _{y=0}$$

$$\tau_{xy} = 0 \Big|_{y=0}$$

$$u = 0 \Big|_{y=d}$$

$$v = 0 \Big|_{y=d}$$

and their transforms are

$$\bar{q} = \left.\begin{array}{ll} \displaystyle\int_{-a}^{a} \left[-q(x)\right] e^{i\omega x}\, dx & (x<a) \\ 0 & (x>a) \end{array}\right| _{y=0}$$

$$\bar{\tau}_{xy} = 0 \Big|_{y=0}$$

$$\bar{u} = 0 \Big|_{y=d}$$

$$\bar{v} = 0 \Big|_{y=d}.$$

Evaluation of arbitrary constants. Evaluating eq A32 for $\bar{\sigma}_y$ at y=0 and eq A33 for $\bar{\tau}_{xy} = 0$ at y=0, yields

$$A_1 + C_1 = -\frac{\bar{q}}{\omega^2} \tag{A36}$$

$$-A_1 + B_1 + C_1 + D_1 = 0. \tag{A37}$$

Evaluating eq A34 and A35 for $\bar{u} = 0$ and $\bar{v} = 0$ respectively, at $y = d$, gives

$$\{A_1 + B_1[\omega d - 2(1 - \nu)]\}e^{-\omega d} + \{C_1 + D_1[\omega d + 2(1 - \nu)]\}e^{\omega d} = 0 \tag{A38}$$

$$\{A_1 + B_1[\omega d + (1 - 2\nu)]\}e^{-\omega d} - \{C_1 + D_1[\omega d - (1 - 2\nu)]\}e^{\omega d} = 0. \tag{A39}$$

The four constants can now be solved from the four simultaneous eq A36 through A39. Eq A38 and A39 can be first divided by $e^{\omega d}$.

$$\begin{vmatrix} 1 & 0 & 1 & 0 \\ -1 & 1 & 1 & 1 \\ e^{-2\omega d} & [\omega d - 2(1-\nu)]e^{-2\omega d} & 1 & [\omega d + 2(1-\nu)] \\ e^{-2\omega d} & [\omega d + (1-2\nu)]e^{-2\omega d} & -1 & [\omega d - (1-2\nu)] \end{vmatrix} \begin{vmatrix} A_1 \\ B_1 \\ C_1 \\ D_1 \end{vmatrix} = \begin{vmatrix} -\bar{q}/\omega^2 \\ 0 \\ 0 \\ 0 \end{vmatrix}$$

Solving for A_1, B_1, C_1, and D_1 results in

$$A_1 = -\frac{\bar{q}}{\omega^2} \frac{(k - 2s^2 + 2s)e^{-2s} - N}{2(k - 2s^2)e^{-2s} - Ne^{-4s} - N} = -\frac{\bar{q}}{\omega^2} A^1 \tag{A40}$$

$$B_1 = -\frac{\bar{q}}{\omega^2} \frac{(2s - 1)e^{-2s} - N}{2(k - 2s^2)e^{-2s} - Ne^{-4s} - N} = -\frac{\bar{q}}{\omega^2} B^1 \tag{A41}$$

$$C_1 = -\frac{\bar{q}}{\omega^2} \frac{(k - 2s^2 - 2s)e^{-2s} - Ne^{-4s}}{2(k - 2s^2)e^{-2s} - Ne^{-4s} - N} = -\frac{\bar{q}}{\omega^2} C^1 \tag{A42}$$

$$D_1 = -\frac{\bar{q}}{\omega^2} \frac{(2s + 1)e^{-2s} + Ne^{-4s}}{2(k - 2s^2)e^{-2s} - Ne^{-4s} - N} = -\frac{\bar{q}}{\omega^2} D^1 \tag{A43}$$

where

$$s = \omega d$$

$$k = -8\nu^2 + 12\nu - 5$$

$$N = 3 - 4\nu.$$

To make the equations dimensionless, $\omega = s/d$ has already been introduced. The following substitutions can also be made:

$$\xi = \frac{y}{d}$$

$$\eta = \frac{x}{d}.$$

General equations. By taking the inverse of eq A31 through A35 in accordance with eq A15, the resulting equations for the stresses and displacements are

$$\sigma_x = \frac{1}{2\pi} \int_{-\infty}^{\infty} \left\{ -\bar{q} \left[(A^1 + B^1[s\xi - 2])e^{-s\xi} + (C^1 + D^1[s\xi + 2])e^{s\xi} \right] \right\} e^{-is\eta} ds \tag{A44}$$

$$\sigma_y = -\frac{1}{2\pi}\int_{-\infty}^{\infty}\left\{-\overline{q}\left[(A^1 + B^1 s\xi)e^{-s\xi} + (C^1 + D^1 s\xi)e^{s\xi}\right]\right\}e^{-is\eta}\,ds \tag{A45}$$

$$\tau_{xy} = \frac{i}{2\pi}\int_{-\infty}^{\infty}\left\{-\overline{q}\left[(-A^1 - B^1[s\xi - 1])e^{-s\xi} + (C^1 + D^1[s\xi + 1])e^{s\xi}\right]\right\}e^{-is\eta}\,ds \tag{A46}$$

$$u = -\frac{(1+\nu)}{2\pi Ei}\int_{-\infty}^{\infty}\left\{-\overline{q}\,\frac{d}{s}\left[(A^1 + B^1[s\xi - 2(1-\nu)])e^{-s\xi}\right.\right.$$

$$\left.\left. + (C^1 + D^1[s\xi + 2(1-\nu)])e^{s\xi}\right]\right\}e^{-is\eta}\,ds \tag{A47}$$

$$v = \frac{(1+\nu)}{2\pi E}\int_{-\infty}^{\infty}\left\{-\overline{q}\,\frac{d}{s}\left[(A^1 + B^1[s\xi + (1-2\nu)])e^{-s\xi}\right.\right.$$

$$\left.\left. - (C^1 + D^1[s\xi - (1-2\nu)])e^{s\xi}\right]\right\}e^{-is\eta}\,ds. \tag{A48}$$

Determining whether the integrands are even or odd (since $e^{-ix} = \cos x - i \sin x$, for an even function the $[i \sin x]$ portion will go to zero, leaving the $[\cos x]$; for an odd function the $[\cos x]$ portion will go to zero, leaving $[i \sin x]$ to replace e^{-ix}), and after checking for symmetry, taking twice the integral from 0 to ∞, the resulting equations are

$$\sigma_x = -\frac{1}{\pi}\int_0^{\infty}\overline{q}\left\{[A^1 + B^1(s\xi - 2)]e^{-s\xi} + [C^1 + D^1(s\xi + 2)]e^{s\xi}\right\}\cos s\eta\,ds \tag{A49}$$

$$\sigma_y = \frac{1}{\pi}\int_0^{\infty}\overline{q}\left\{[A^1 + B^1 s\xi]e^{-s\xi} + [C^1 + D^1 s\xi]e^{s\xi}\right\}\cos s\eta\,ds \tag{A50}$$

$$\tau_{xy} = \frac{1}{\pi}\int_0^{\infty}\overline{q}\left\{[-A^1 - B^1(s\xi - 1)]e^{-s\xi} + [C^1 + D^1(s\xi + 1)]e^{s\xi}\right\}\sin s\eta\,ds \tag{A51}$$

$$u = -\frac{(1+\nu)d}{\pi E}\int_0^{\infty}\frac{\overline{q}}{s}\left\{[A^1 + B^1(s\xi - 2[1-\nu])]e^{-s\xi}\right.$$

$$\left. + [C^1 + D^1(s\xi + 2[1-\nu])]e^{s\xi}\right\}\sin s\eta\,ds \tag{A52}$$

$$v = -\frac{(1+\nu)\,d}{\pi E}\int_0^\infty \frac{\bar{q}}{s}\Big\{[A^1 + B^1(s\xi + [1-2\nu])]e^{-s\xi}$$

$$- [C^1 + D^1(s\xi - [1-2\nu])]e^{s\xi}\Big\}\cos s\eta\, ds \tag{A53}$$

where

$$A^1 = \frac{(k - 2s^2 + 2s)\,e^{-2s} - N}{[\mathrm{DEN}]}$$

$$B^1 = \frac{(2s-1)\,e^{-2s} - N}{[DEN]}$$

$$C^1 = \frac{(k - 2s^2 - 2s)\,e^{-2s} - N\,e^{-4s}}{[DEN]}$$

$$D^1 = \frac{(2s+1)\,e^{-2s} + N\,e^{-4s}}{[DEN]}$$

in which

$$[DEN] = 2(k - 2s^2)\,e^{-2s} - N\,e^{-4s} - N. \tag{A54}$$

Considering now the method used in conducting the laboratory tests, it is necessary to establish that the stress factor $\bar{q}$ at the surface-load interface in eq A49-A53 is compatible with the manner in which the load was applied; in this case it was a rigid plate or stamp.

First, the expression for vertical deflection, eq A53, has to be evaluated at $y = 0$. Substituting $s = \omega d$, $\xi = y/d$ and $\eta = x/d$ back into eq A53 gives

$$v = -\frac{(1+\nu)}{\pi E}\int_0^\infty \frac{1}{\omega}\Big[(A^1 + B^1[\omega y + (1-2\nu)])\,e^{-\omega y}$$

$$- (C^1 + D^1[\omega y - (1-2\nu)])\,e^{\omega y}\Big]\bar{q}\cos\omega x d\omega.$$

Then

$$v\Big|_{y=0} = -\frac{(1+\nu)}{\pi E}\int_0^\infty \frac{1}{\omega}\Big[A^1 + B^1(1-2\nu) - C^1 + D^1(1-2\nu)\Big]\bar{q}\cos\omega dx\omega.$$

Letting

$$\bar{q} = \frac{\omega J_0(\omega a)}{A^1 - C^1 + (B^1 + D^1)(1-2\nu)}$$

where $J_0(\omega a)$ = Bessel function;[24] and since from eq A37

$$A^1 - C^1 = B^1 + D^1$$

then

$$\overline{q} = \frac{\omega J_0(\omega a)}{2(1 - \nu)(B^1 + D^1)}. \tag{A55}$$

Therefore, the component of displacement in the y direction satisfies the relation

$$\left.\frac{\partial v}{\partial x}\right|_{y=0} = -\frac{(1 + \nu)}{\pi E} \int_0^\infty J_0(\omega a)(-\sin \omega x)\, d\omega$$

so that

$$\left.\frac{\partial v}{\partial x}\right|_{y=0} = \begin{cases} 0 & (-a < x < a) \\ \dfrac{(1 + \nu)}{\pi E(x^2 - a^2)^{1/2}} & (-a > x > a) \end{cases}$$

showing that v is constant along the strip $-a < |x| < a$ of the boundary $y = 0$, as shown by Sneddon.[24]

The nondimensionalized expression for $\overline{q}$, eq A55, becomes

$$\overline{q} = \frac{J_0(s\alpha)s}{2d(1 - \nu)(B^1 + D^1)} \tag{A56}$$

where

$$\alpha = \frac{a}{d}.$$

It can be seen that by substituting eq A56 into eq A49 through A53, the denominator for the arbitrary constants, eq A54, cancels out, and the general equations for stresses and deformations now become

$$\sigma_x = -\frac{1}{2\pi d(1 - \nu)} \int_0^\infty J_0(s\alpha)s\left[\frac{(A + B[s\xi - 2])\, e^{-s\xi} + (C + D[s\xi + 2])\, e^{s\xi}}{B + D}\right]\cos s\eta\, ds \tag{A57}$$

$$\sigma_y = \frac{1}{2\pi d(1-\nu)} \int_0^\infty J_0(s\alpha)s \left[\frac{(A + Bs\xi)e^{-s\xi} + (C + Ds\xi)e^{s\xi}}{B + D} \right] \cos s\eta \, ds \tag{A58}$$

$$\tau_{xy} = \frac{1}{2\pi d(1-\nu)} \int_0^\infty J_0(s\alpha)s \left[\frac{(-A - B[s\xi - 1])e^{-s\xi} + (C + D[s\xi + 1])e^{s\xi}}{B + D} \right] \sin s\eta \, ds \tag{A59}$$

$$u = -\frac{(1+\nu)}{2\pi E(1-\nu)} \int_0^\infty J_0(s\alpha) \left[\frac{(A + B[s\xi - 2(1-\nu)])e^{-s\xi}}{B + D} + \frac{(C + D[s\xi + 2(1-\nu)])e^{s\xi}}{B + D} \right] \sin s\eta \, ds \tag{A60}$$

$$v = -\frac{(1+\nu)}{2\pi E(1-\nu)} \int_0^\infty J_0(s\alpha) \left[\frac{(A + B[s\xi + (1-2\nu)])e^{-s\xi}}{B + D} - \frac{(C + D[s\xi - (1-2\nu)])e^{s\xi}}{B + D} \right] \cos s\eta \, ds \tag{A61}$$

where

$$A = (k - 2s^2 + 2s)e^{-2s} - N$$

$$B = (2s - 1)e^{-2s} - N$$

$$C = (k - 2s^2 - 2s)e^{-2s} - Ne^{-4s}$$

$$D = (2s + 1)e^{-2s} + Ne^{-4s}$$

$$k = -8\nu^2 + 12\nu - 5$$

$$N = 3 - 4\nu$$

and

$$s = \omega d$$

$$\xi = \frac{y}{d}$$

$$\eta = \frac{x}{d}$$

$$\alpha = \frac{a}{d}$$

E = Young's modulus

ν = Poisson's ratio.

Solution of eq A57-A61 by numerical integration would yield expressions representing the elastic case.

The viscoelastic stress-strain relations for snow are not known. However, by selecting a rheological model which would approximate the behavior of snow, proper substitutions for the elastic constants could be made.

The relationships between the elastic constants are

$$\text{Shear modulus: } G = \frac{E}{2(1 + \nu)}$$

$$\text{Bulk modulus: } K = \frac{E}{3(1 - 2\nu)}$$

$$\text{Poisson's ratio: } \nu = \frac{2k - 2G}{6K + 2G}.$$

In the viscoelastic case, a plausible model for the bulk modulus would be a spring in series with a Voigt model, and for the shear modulus a Maxwell model in series with a Voigt model. The validity of these assumptions could be checked by comparing the theoretical solutions with experimental data. Various models could be tried until some agreement between theory and experimental data is obtained. Poisson's ratio for snow is not well established; however, reasonable estimates could be obtained from available data (see Fig. 8).

When solving eq A57-A61, it becomes apparent that the equations are not satisfactory since they do not yield acceptable solutions. When the equations are integrated, the value of the integrand approaches infinity. It is quite likely that the boundary conditions may have been assumed incorrectly.

Apparently this sort of difficulty has been encountered before. In the case of an infinite strip load on a semi-infinite elastic medium for both a uniformly distributed load (Michell's solution) and a rigid plate (Sadowsky's solution),[25] the vertical displacements in both solutions approach infinity as the vertical coordinate approaches infinity (v increases as log γ).[10] Therefore, the validity of the solutions for displacements in this problem is also questionable.

The development of the equations, therefore, was discontinued at this point and is included here for reference only.

APPENDIX B. TEST DATA AND CALCULATIONS

Table BI. Snow sample strength data.

Test no.	*Bearing plate size, L (in.)*	*Snow type**	*Age (days)*	*Density γ (g/cm^3)*	*Unconfined compressive strength σ_u (psi)*	*Bearing strength (confined) σ_i (psi)*	*Remarks*
0	4	N-c	5	0.374	11.8	22	Trial test, no photos
1	4	P-c	34	.565	134		Of doubtful reliability†
2	8	P-nc	68	.533	98	121	Of doubtful reliability†
3	6	P-c	68	.542 .542	76.8 63.9	110	
4	4	P-c	70	.592	130	171	
5	4	P-nc	17	.466 .451	- 77.9	97.6	
6	4	P-nc	17	.420	34	43.7	
7	6	P-c	70	.562	125	164	
8	8	P-nc	25	.439 .442	28.7 29.9	41	
9	6	P-nc	25	.461 .440 .446	74.6 44.9 -	85	
10	6	P-nc	27	.474 .473	52 52	81.9	Of doubtful reliability†
12	10	P-nc	29	.444	39.9	43.7	
13	6	N-c	31	.375 .378 .385	8.2 8.3 10.5	18.2	
14	8	N-c	31	.384 .378	14.7 9.6	19.1	
15	10	N-nc	38	.284 .315	3.2 4.6	7.7	
16	4	N-nc	38	.342 .337	5.3 3.2	10.9	
17	8	N-nc	38	.312 .307	7.6 3.2	9.1	
18	8	N-c	42	.356 .358	6.4 10.9	13.7	

*N = Natural snow
P = Processed snow
nc = Not compacted
c = Compacted

†Some slipping of the sample inside the container occurred during the test; sample not cut with sufficient accuracy to insure a perfect fit in container.

Table BII. Snow sample strength data (composite samples).

Test no.	Age (days)		Thickness of processed layer (in.)	Density (g/cm^3)		Unconfined compressive strength σ_u (psi)		Bearing strength (confined) σ_i (psi)
	Processed	Natural		Processed	Natural	Processed	Natural	
19	75	50	6	0.546 .540 .537	0.398 .404 .406	126 83 105	25.6 43 35.7	68.3
20	75	50	4	.540 .541	.387 .400	124.5 102	23.2 19.6	53
21	85	60	5	.521	.373	96	14.2	55.5
23	85	60	8	.520	.370			82

Snow type: Processed-compacted on Natural-compacted
Bearing plate size: 4 in.

Table BIII. Additional density-strength data.

Snow type	Age (days)	Density (g/cm^3)	Unconfined compressive strength (psi)
Processed, compacted	68	0.502	58.5
	68	.542	63.9
Processed, not compacted,	17	.466	90.5
	25	.466	40.8
	25	.442	41.6
	25	.440	29.3
	25	.459	43.9
	25	.443	36.5
	25	.446	35.4
	25	.442	37.4
	25	.443	83.4
	29	.465	53.0
Natural, compacted	31	.364	7.6
	31	.395	16.6
	38	.354	11.7

Table BIV. Bearing strength (confined) vs unconfined strength (from Table BI).

Test no.	*Unconfined** σ_u *(psi)*	*Confined* σ_i *(psi)*
	X	Y
15	3.9	7.7
16	4.2	10.9
17	5.4	9.1
18	8.6	13.7
13	9.0	18.2
0	11.8	22.0
14	12.1	19.1
8	29.3	41.0
6	34.0	43.7
12	39.9	43.7
10	52.0	81.9
9	59.8	85.0
3	76.8	110.0
5	77.9	97.6
2	98.0	121.0
-†	114.0	137.0
7	125.0	164.0
4	130.0	171.0

$$\sigma_i = m\sigma_u + b$$

$$(Y = mx + b)$$

$$n = 18$$

$$M_x = 49.1$$

$$M_y = 66.5$$

$$m = \frac{\Sigma xy - nM_xM_y}{\Sigma x^2 - n(M_x)^2} = 1.24$$

$$b = M_y - mM_x = 5.60$$

$$Y = 1.24X + 5.6$$

$$\sigma_i = 1.24\sigma_u + 5.6$$

Coefficient of correlation:

$$r = \left\{ \frac{(n\Sigma xy - \Sigma x\Sigma y)^2}{[n\Sigma x^2 - (\Sigma x)^2]\,[n\Sigma y^2 - (\Sigma y)^2]} \right\}^{1/2} = 0.99.$$

Standard error of estimate:

$$s_{x,y} = \left[\frac{\Sigma y^2 - b\Sigma y - m\Sigma xy}{n} \right]^{1/2} = 4.6 \text{ (psi)}.$$

*Where more than one unconfined compressive strength test was performed for each confined strength test, the mean value was used.

†From a preliminary equipment check-out test.

Table BV. Sieve analysis data.

Snow type	*Processed, compacted*			*Natural, not compacted*		
Test	*Test A*	*Test B*	*Mean*	*Test C*	*Test D*	*Mean*
Snow density (g/cm³)	0.543	0.550	-	0.330	0.329	-
Sample size (g)	296.8	256.6	-	204.5	280.3	-
Sieve no.			*% Finer*			
4	99.9	98.8	99.4	100.0	100.0	100.0
10	98.8	93.6	96.2	100.0	100.0	100.0
20	79.9	65.9	72.9	95.0	99.4	97.2
40	42.5	33.6	38.0	68.3	72.7	70.5
60		(not used)		22.7	19.3	21.0
80	8.5	9.2	8.9	5.45	5.0	5.2
120	1.8	1.8	1.8	0.95	0.6	0.8
200	0.15	0.1	0.12	0	0	0
	$C_u = \frac{D_{60}}{D_{10}} = 3.2$			$C_u = \frac{D_{60}}{D_{10}} = 1.9$		
	$M = D_{50} = 0.49$ mm			$M = D_{50} = 0.35$ mm		

The relative particle size distribution in the natural and processed snows is shown in Figure B1.

A very convenient method of indicating the particle size distribution is by plotting the data on a log-probability graph, as shown in Figure B2. From this, the parameters which characterize the nature of the distribution, such as the geometric mean diameter (by weight) and the geometric standard deviation (by weight), may be obtained if the plot yields a straight line.[26]

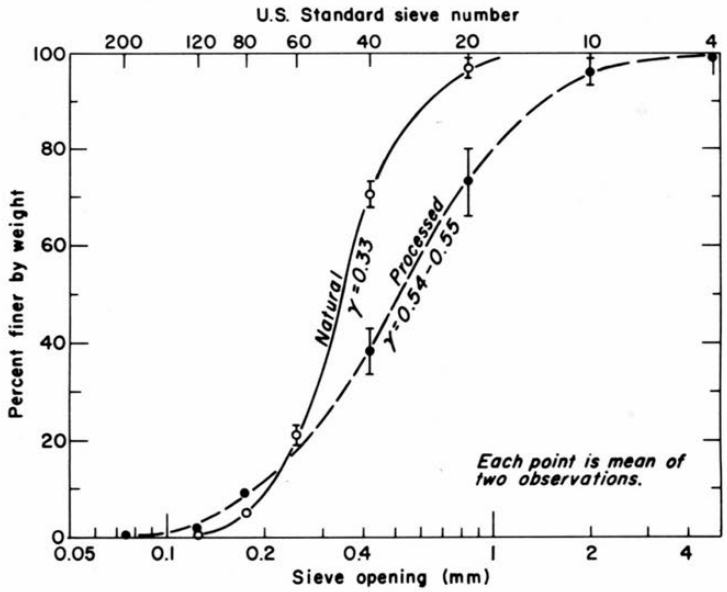

Figure B1. Particle size distribution.

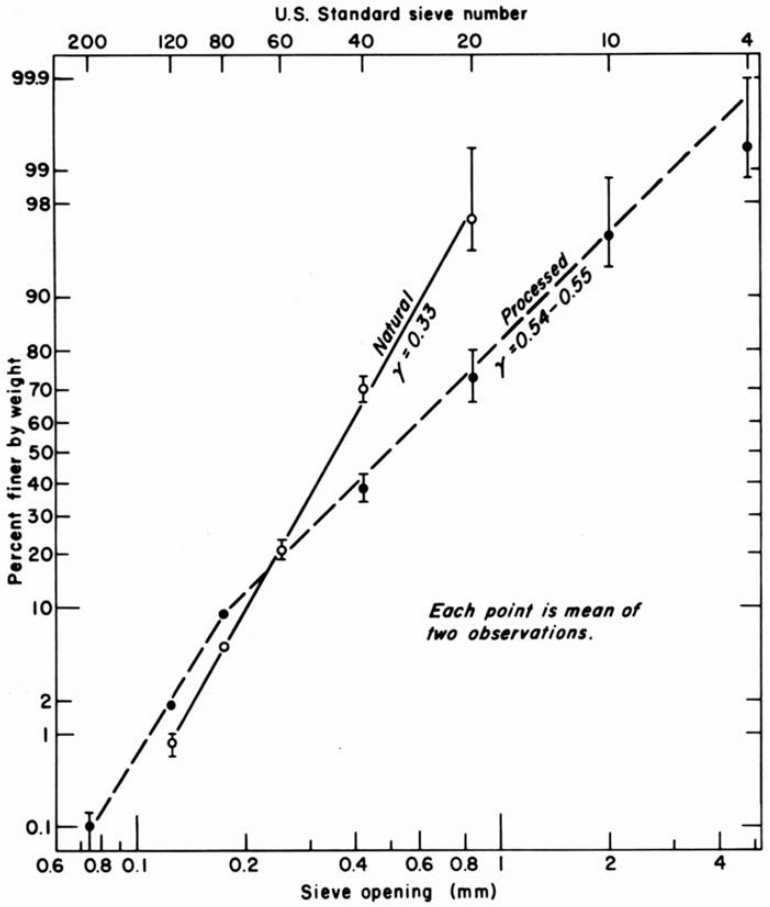

Figure B2. Particle size distribution (log-probability plot).

Table BVI. Density-sinkage-bearing strength data at initial failure.

Test no.	Density γ (g/cm^3)	Plate size r (in.)	Sinkage z (in.)	Bearing strength σ_i (psi)	s/r	Relative density ($\gamma_{snow}/\gamma_{ice}$)	Density numeric ($\gamma_{snow}/\gamma_{ice}$)/$C_r$
15	0.30	5	0.65	7.7	0.130	0.327	0.47
17	.31	4	.68	9.2	.170	.338	.43
16	.34	2	.52	10.9	.260	.371	.37
18	.357	4	.65	13.7	.163	.389	.49
13	.381	3	.35	18.2	.117	.415	.48
14	.381	4	.50	19.1	.125	.415	.53
6	.420	2	.35	43.7	.175	.458	.46
8	.440	4	.23	41.0	.057	.480	.61
12	.440	5	.30	43.7	.060	.480	.69
9	.446	3	.22	85.0	.073	.483	.56
5	.458	2	.28	97.6	.140	.500	.50
10	.473	3	.25	81.9	.083	.516	.59
2	.533	4	.23	121.0	.057	.581	.74
3	.542	3	.20	110.0	.066	.591	.68
7	.562	3	.22	164.0	.073	.613	.71
4	.592	2	.11	171.0	.055	.645	.65

$r = \frac{1}{2}L$

$\gamma(ice) = .917$

r	C_r
2	1.0
3	.87
4	.79
5	.70

Table BVII. Pressure-sinkage-photograph data.

Test no.	Plate size L (in.)	Density γ (g/cm^3)	Photo no.	Pressure p (psi)	Sinkage z (in.)	k_1	Computed p_m	η	χ
15	10	0.30	6-23	0	0	44	8.8	-	-
			6-25	5.5	0.20			1.00	0.62
			6-25A	6.0	.28			1.40	.68
			6-26	7.0	.41			2.05	.80
			6-27	7.7	.65			3.25	.88
17	8	.31	6-29	0	0	46	10.8	-	-
			6-29A	3.0	.07			0.39	.28
			6-30	5.6	.22			1.22	.52
			6-30A	7.0	.28			1.56	.65
			6-31	9.1	.44			2.45	.85
			6-36	9.2	.68			3.78	.86
16	4	.34	6-18	0	0	65	13.5	-	-
			6-19	8.2	.20			0.96	.61
			6-19A	10.0	.30			1.44	.74
			6-20	10.5	.40			1.93	.78
			6-22	10.9	.52			2.50	.81
18	8	.357	2-2	0	0	80	15.3	-	-
			2-2A	6.0	.10			0.48	.39
			2-4	9.6	.17			0.82	.61
			2-5	10.9	.35			1.68	.70
			2-6	12.3	.50			2.40	.79
			2-7	13.7	.65			3.12	.88
13	6	.381	6-4	0	0	110	23.6	-	-
			6-5	10.9	.10			0.44	.45
			6-5A	14.0	.15			0.66	.58
			6-6A	17.0	.25			1.10	.70
			6-7	18.2	.35			1.54	.75
14	8	.381	6-10	0	0	110	23.6	-	-
			6-11	9.6	.15			0.66	.40
			6-12	15.3	.30			1.32	.63
			6-13A	17.0	.40			1.76	.70
			6-16	19.1	.50			2.20	.79
6	4	.42	3-20	0	0	240	62.8	-	-
			3-22	28.6	.15			0.61	.47
			3-22A	34.0	.20			0.82	.55
			3-23A	41.0	.30			1.22	.67
			3-24	43.7	.35			1.43	.71
			3-25	< 40.0	.60			-	-
			3-28	< 50.0				-	-
8	8	.44	4-5	0	0	330	64.0	-	-
			4-9	21.9	.08			0.42	.35
			4-11	34.1	.14			0.74	.54
			4-11A	38.0	.18			0.95	.60
			4-12	41.0	.23			1.21	.65
			4-17	< 41.0	.45			-	-
12	10	.44	5-19	0	0	330	64.0	-	-
			5-21	21.8	.07			0.37	.34
			5-22	38.2	.15			0.79	.60
			5-23A	41.0	.20			1.05	.65
			5-25	43.7	.30			1.58	.69
			5-26	< 40.0	.40			-	-

Table BVII (Cont'd). Pressure-sinkage-photograph data.

Test no.	Plate size L (in.)	Density γ (g/cm^3)	Photo no.	Pressure p (psi)	Sinkage z (in.)	k_1	Computed p_m	η	χ
9	6	0.446	4-20	0	0	385	∞*		
			4-23	51.0	.13				
			4-24	63.8	.17				
			4-27	85.0	.22				
			4-28	< 85.0	.35				
			4-34	< 85.0	.50				
5	4	.458	3-5	0	0	353	∞		
			3-8	53.7	.15				
			3-9	97.6	.28				
			3-10	< 80.0	.45				
			3-12	< 90.0	.75				
10	6	.473	5-6	0	0	348	∞		
			5-8	36.4	.10				
			5-10	63.8	.18				
			5-12	69.1	.20				
			5-15	81.9	.25				
2	8	.533	2-10	0	0	517	∞		
			2-12	76.0	.15				
			2-13	121.0	.23				
			2-14	<120.0	.35				
3	6	.542	2-16	0	0	576	∞		
			2-17	60.1	.10				
			2-18	110.0	.20				
			2-19	<100.0	.45				
7	6	.562	2-29	0	0	773	∞		
			2-30	36.4	.05				
			2-31	91.0	.12				
			2-32	129.0	.15				
			2-33	164.0	.22				
			2-34	<140.0	.32				
			2-35	<160.0	.38				
			2-36	<160.0	.45				
4	4	.592	2-21	0	0	1551	∞		
			2-22	27.3	.015				
			2-23	54.6	.038				
			2-24	82.0	.060				
			2-25	137.0	.087				
			2-26	171.0	.11				
			2-27	<150.0	.20				
			2-28	<170.0	.40				
	Composite Samples								
19	4	.54 / .40	7-2	0	0				
			7-3	13.7	.05				
			7-4	32.0	.10				
			7-5	54.0	.17				
			7-6	68.3	.22				
			7-7	< 60.0	.33				

*Calculated $p_m = \infty$ because of a linear z vs p relationship up to the initial failure point and is, therefore, representative of the material behavior only up to that point.

Table BVII (Cont'd). Pressure-sinkage-photograph data.

Test no.	Plate size L (in.)	Density γ (g/cm^3)	Photo no.	Pressure p (psi)	Sinkage z (in.)	k_1	Computed p_m	η	χ
20	4	0.54 / 0.39	7-10	0	0				
			7-11	13.7	.05				
			7-12	21.8	.10				
			7-13	35.5	.15				
			7-14	53.0	.24				
			7-16	< 50.0	.37				
			7-17	< 50.0	.45				
21	4	.52 / .37	8-1	0	0				
			8-3	24.1	.10				
			8-4	37.3	.15				
			8-5	55.5	.23				
			8-6	< 50.0	.40				
23	4	.52 / .37	8-10	0	0				
			8-11	27.3	.07				
			8-12	41.0	.13				
			8-13	65.0	.18				
			8-14	82.0	.24				
			8-15	< 80.0	.50				

APPENDIX C. SELECTED, REPRESENTATIVE PHOTOGRAPHS

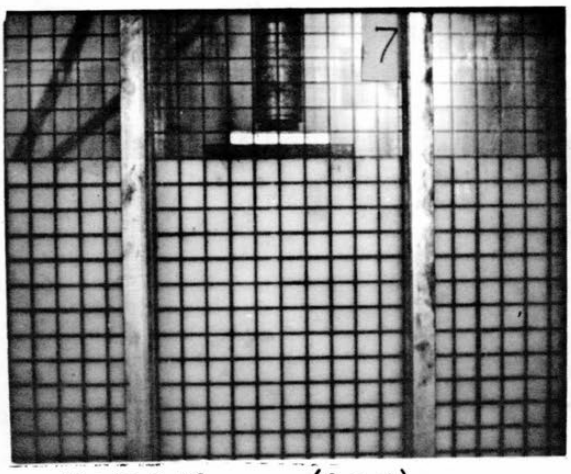

Photo 2-29 (0 psi)

Photo 2-31 (91 psi)

Photo 2-33 (164 psi, failure)

Photo 2-35 (< 150 psi)

Photo 2-36 (< 150 psi)

TEST NO: 7

Snow: Processed, compacted

Density: .56 g/cm^3

Age: 70 days

Bearing plate: 6 in.

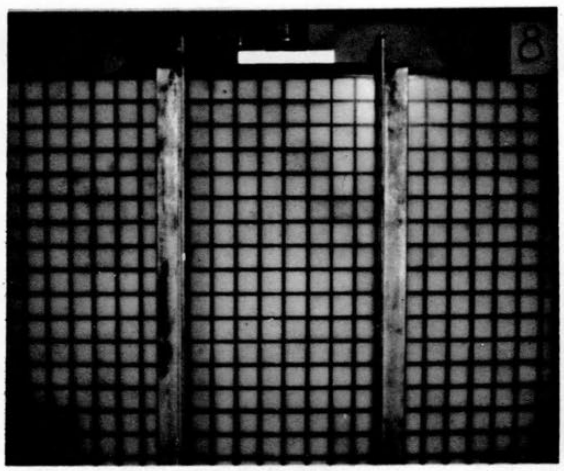

Photo 4-5 (0 psi)

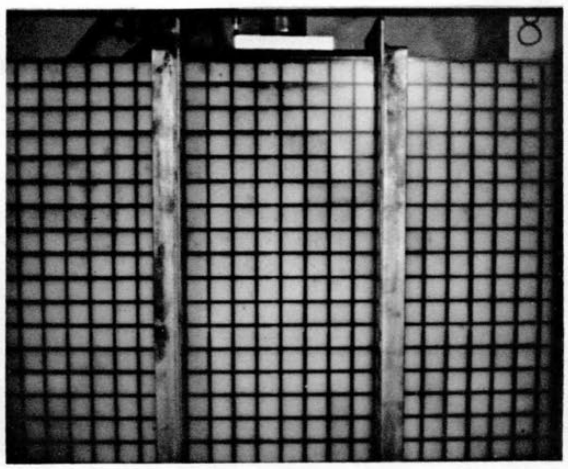

Photo 4-11 (34.1 psi)

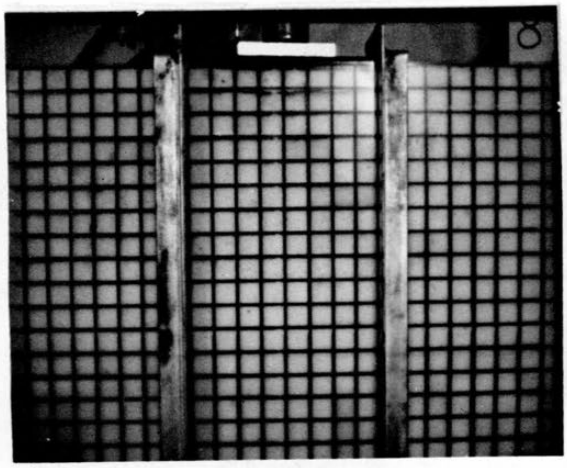

Photo 4-12 (41 psi, failure)

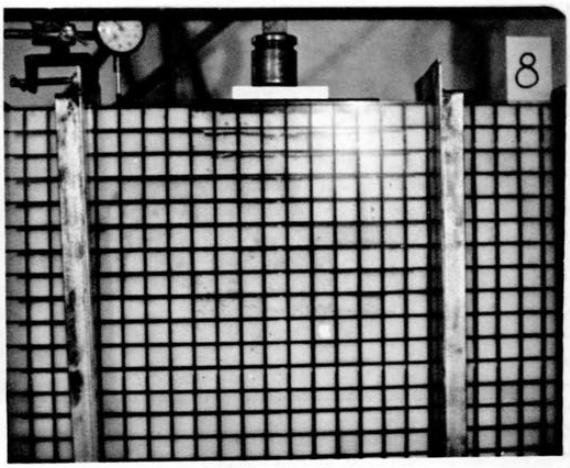

Photo 4-15 (41 psi)

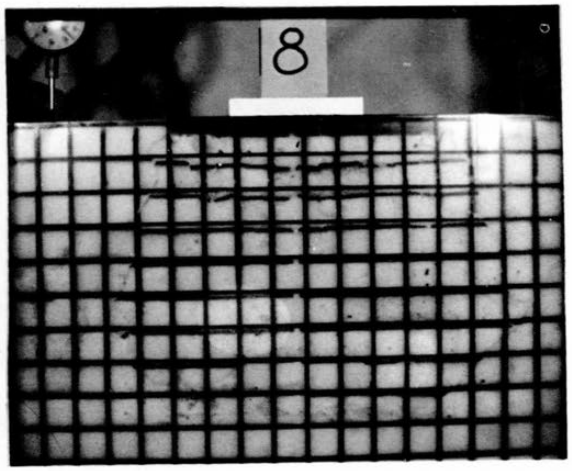

Photo 4-17 (41 psi)

TEST NO: 8

Snow: Processed, not compacted

Density: .44 g/cm^3

Age: 25 days

Bearing Plate: 8 in.

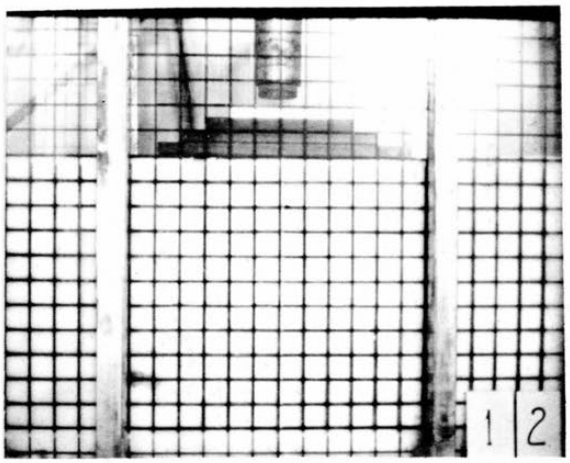

Photo 5-19 (0 psi)

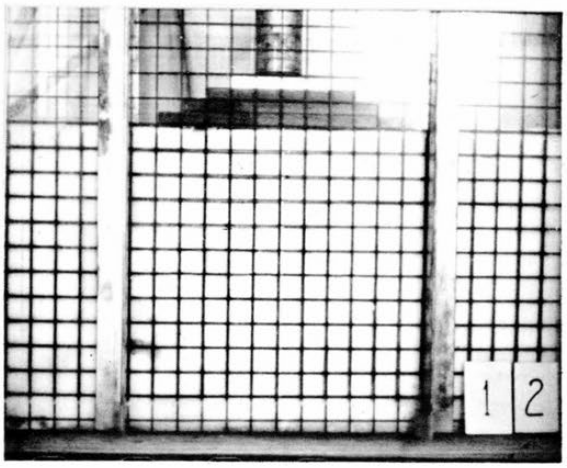

Photo 5-21 (21.8 psi)

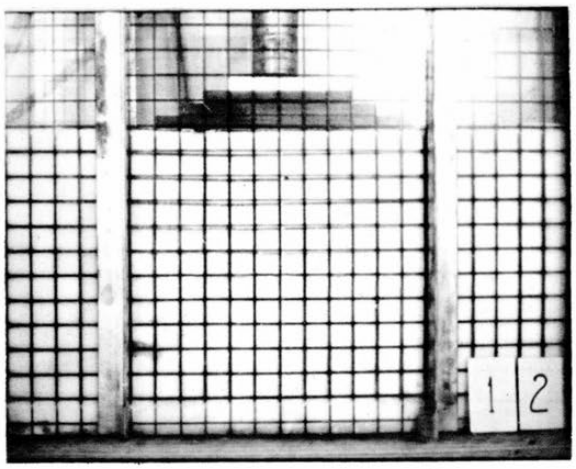

Photo 5-22 (38.2 psi)

Photo 5-25 (43.7 psi, failure)

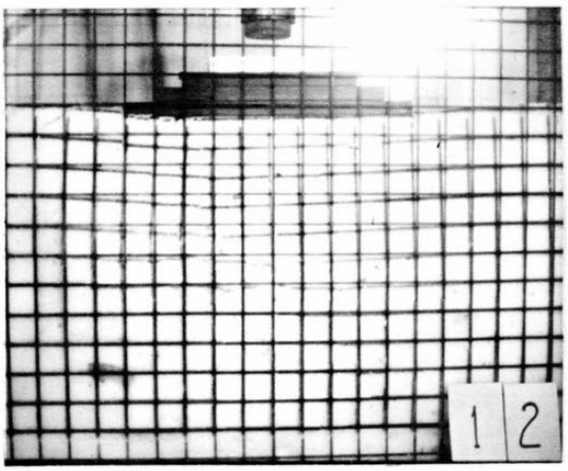

Photo 5-26 (48.7 psi)

TEST NO: 12

Snow: Processed, not compacted

Density: .44 g/cm^3

Age: 29 days

Bearing plate: 10 in.

Photo 6-29 (0 psi)

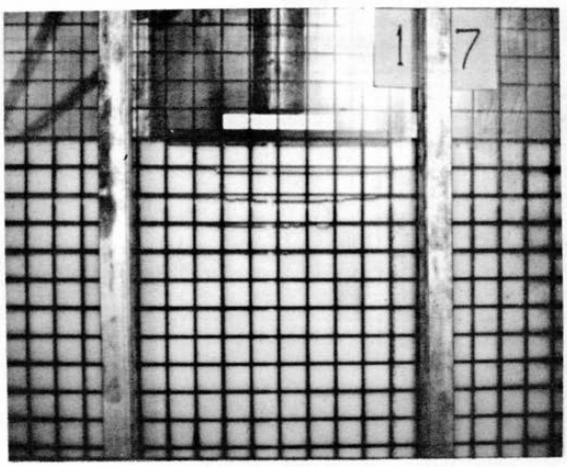

Photo 6-30 (5.6 psi)

Photo 6-31 (9.1 psi, failure)

Photo 6-36 (9.2 psi)

TEST NO: 17

Snow: Natural, not compacted

Density: .31 g/cm^3

Age: 38 days

Bearing plate: 8 in.

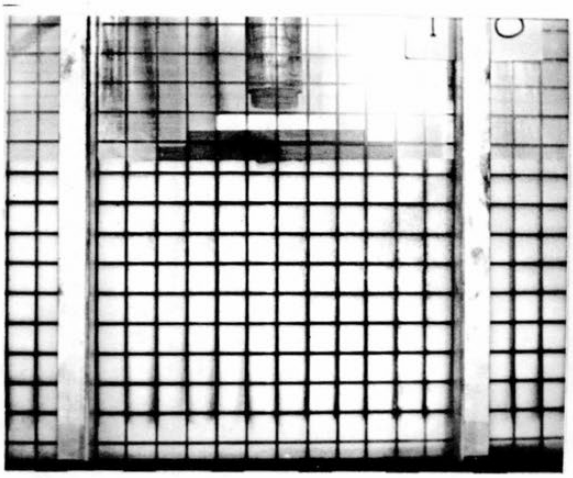

Photo 2-2 (0 psi)

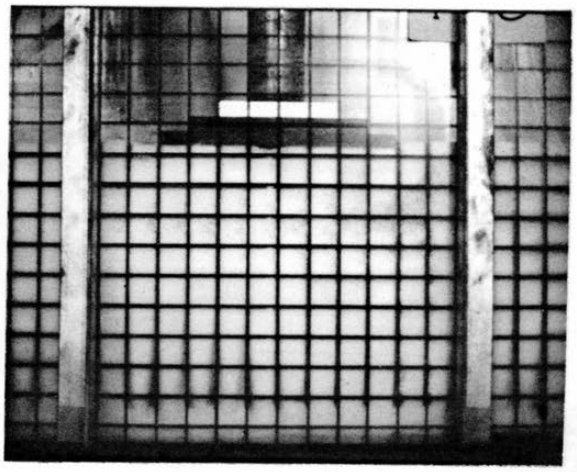

Photo 2-4 (9.6 psi)

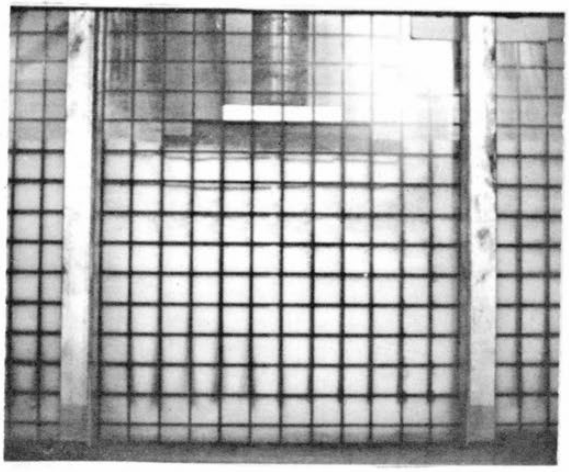

Photo 2-5 (10.9 psi)

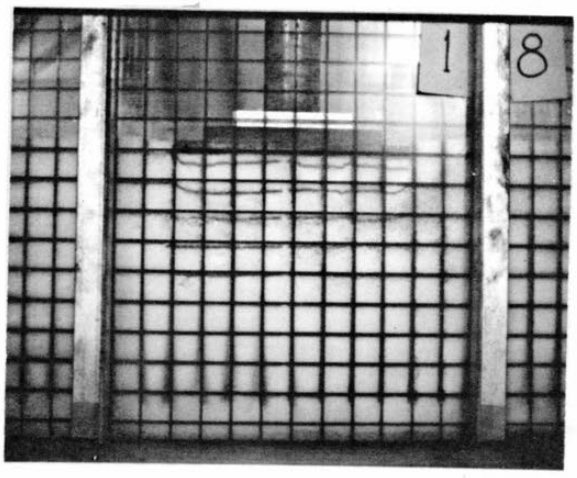

Photo 2-6 (12.3 psi)

Photo 2-7 (13.7 psi, failure)

TEST NO: 18

Snow: Natural, compacted
Density: .36 g/cm^3
Age: 42 days
Bearing plate: 8 in.

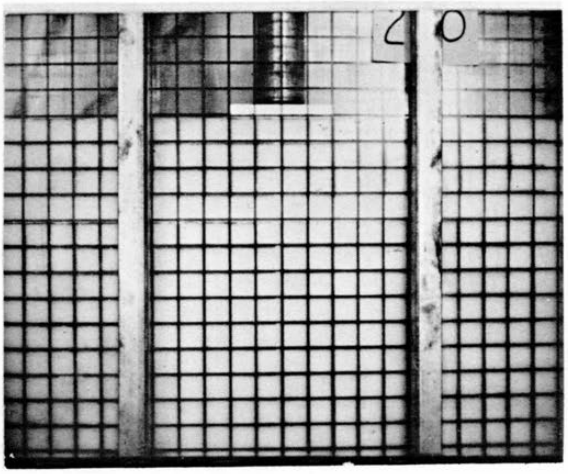

Photo 7-12 (21.8 psi)

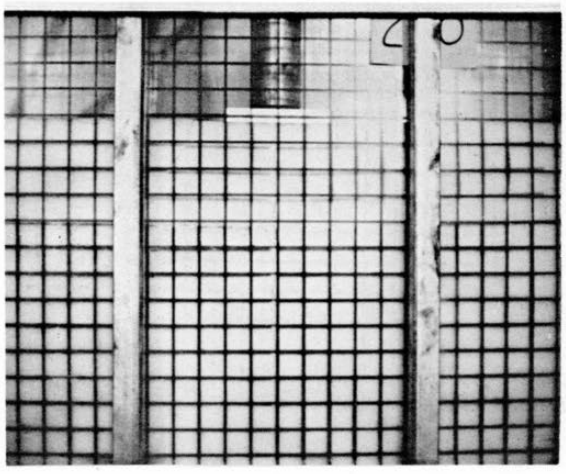

Photo 7-14 (53 psi, failure)

Photo 7-16 (< 50 psi)

Photo 7-17 (< 50 psi)

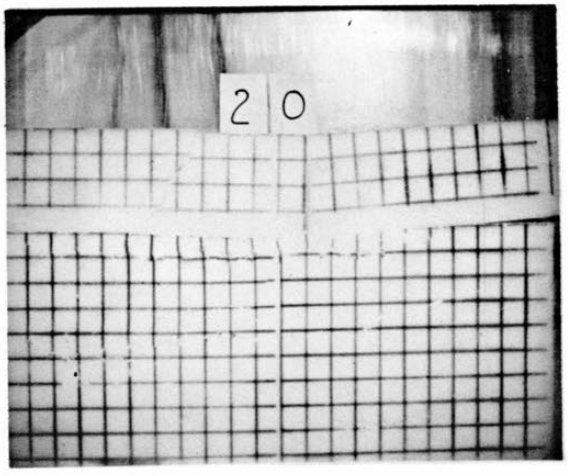

Photo 7-21 (same as 7-17)

TEST NO: 20

Snow: Composite sample, 4 in. of processed snow on top of natural snow

Density, processed: .54 g/cm^3
natural: .39 g/cm^3

Age, processed: 75 days
natural: 50 days

Bearing plate: 4 in.

APPENDIX D. SCHEDULE OF TESTS PERFORMED

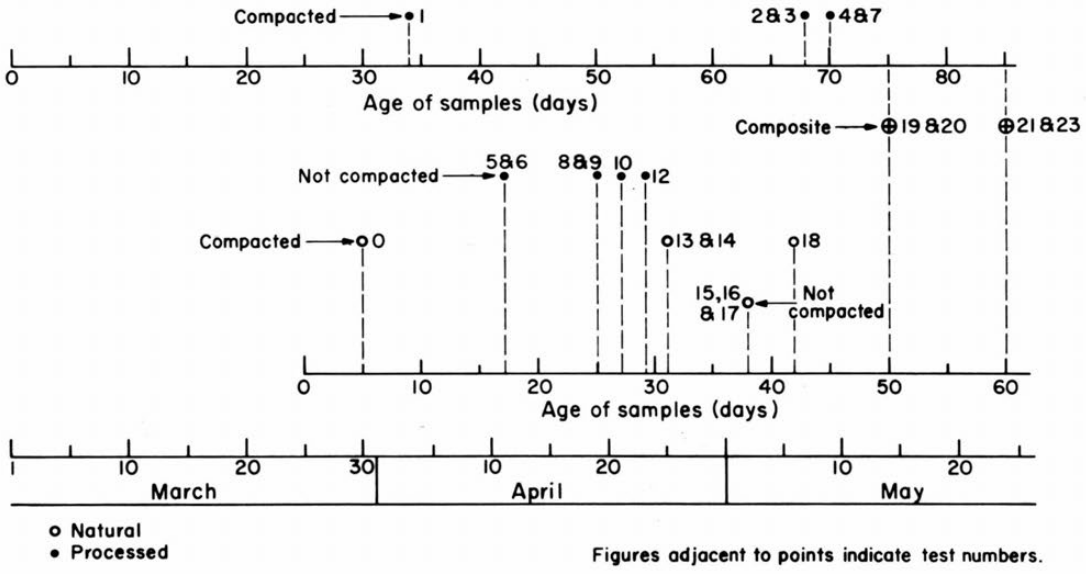

DOCUMENT CONTROL DATA - R & D

(Security classification of title, body of abstract and indexing annotation must be entered when the overall report is classified)

1. ORIGINATING ACTIVITY *(Corporate author)*
U. S. Army Cold Regions Research and Engineering Laboratory
Hanover, New Hampshire 03755

2a. REPORT SECURITY CLASSIFICATION
Unclassified

2b. GROUP

3. REPORT TITLE

DEFORMATION OF SNOW UNDER RIGID PLATES AT A CONSTANT RATE OF PENETRATION

4. DESCRIPTIVE NOTES *(Type of report and inclusive dates)*

5. AUTHOR(S) *(First name, middle initial, last name)*

Gunars Abele

6. REPORT DATE: March 1970

7a. TOTAL NO. OF PAGES: 70

7b. NO. OF REFS: 88

8a. CONTRACT OR GRANT NO.

b. PROJECT NO.

c. DA Task 1T062112A13001

d.

9a. ORIGINATOR'S REPORT NUMBER(S)
Research Report 273

9b. OTHER REPORT NO(S) *(Any other numbers that may be assigned this report)*

10. DISTRIBUTION STATEMENT
This document has been approved for public release and sale; its distribution is unlimited

11. SUPPLEMENTARY NOTES

12. SPONSORING MILITARY ACTIVITY
U. S. Army Cold Regions Research and Engineering Laboratory
Hanover, New Hampshire 03755

13. ABSTRACT
This report presents the results of a study performed on the behavior, particularly the deformation, of snow under a load applied to a rigid plate at a constant rate of penetration. The results will eventually be used in the development of design criteria for snow roads, runways, and foundations in the polar regions. The tests were conducted on snow samples having a high width/length ratio, simulating a two-dimensional case. The effect of snow density, plate size, and pressure on the deformation of snow below the load was investigated. The pressure-sinkage relationships and the bearing strength as functions of density were also investigated. It was determined that density, in the range 0.3 to 0.6 g/cm^3, can be used as a reasonably reliable index for predicting deformation and behavior of snow under load. In general, the critical pressure (bearing strength) increased as a power function of density, and critical sinkage decreased as a power function of density. It was also observed that the deformation bulb resembled the typical Boussinesq stress bulb. The experimental pressure-sinkage relationships agreed closely with recently developed theoretical values. For the range of plate sizes used, the test data did not provide conclusive evidence of the effect of plate size on deformation and bearing capacity of snow. The possibility of using the Moiré fringe method for determing deformation patterns in snow and soils under various loading conditions should be investigated.

14. Key Words: Bearing strength, Deformation, Density measurements, Penetration tests, Snow mechanics

DD FORM 1 NOV 68 1473 REPLACES DD FORM 1473, 1 JAN 64, WHICH IS OBSOLETE FOR ARMY USE.